To Investigate the Effect of Bolus On Skin Dose in VMAT/IMRT For Head and Neck Cancer

A thesis submitted in partial fulfilment of the requirements for the Degree

of Master of Science in Medical Physics

by

Chitra J. Shenoy

Department of Physics and Astronomy
University of Canterbury
Christchurch, New Zealand

2016

Contents

Acknowledgements

First and foremost I am grateful to my supervisor Laura Ciurlionis, my thesis supervisor within the Auckland City Hospital, for her constant support and advice.

I owe my deepest gratitude to my supervisor at University of Canterbury, Dr. Steven Marsh, for his support and guidance throughout this thesis.

I would like to express my gratitude to my many colleagues for being accessible and willing to answer my endless questions. I would like to specially thank Dr. Gerard Bengua, Fiona Bignell, and Allan Stewart.

Last but not the least, I would like to thank my husband, Jayesh , my sons, Manjunath and Adinath, for their encouragement and support throughout the duration of project.

Abstract

External beam radiotherapy is used to treat the postsurgical bed of primary tumours and regional lymph nodes in head and neck cancer treatment. As megavoltage photons have a skin sparing effect, bolus is used to provide dose build-up and deliver high doses to scar tissue on the skin.

At the Radiation Oncology Department of Auckland City Hospital (ACH) IMRT and VMAT are used to treat these patients. This work investigates whether bolus material is necessary to ensure that the scars on the skin of head and neck radiotherapy patients receive an adequate dose of radiation.

A retrospective planning study was performed to investigate whether clinically acceptable IMRT and VMAT plans could be developed to deliver full dose to the scar tissues without bolus. It was possible to generate excellent PTV coverage in all cases without bolus, but doses to the scar tissue were on average 12% lower than those produced in the original plans. The results of this study were verified with a phantom study and film dosimetry.

Surface dose in the original plan with bolus measured with film was in good agreement with the dose predicted by Pinnacle^3. However, there was considerable discrepancy in measured and predicted surface doses for the no bolus plans. Pinnacle^3 overestimated the surface doses in no bolus plans.

If the goal is to adequately treat the scar tissue whilst maintaining a good quality dose distribution within the target, this study demonstrates that bolus is a necessary component of the treatment delivery process.

List of Figures

List of Tables

Glossary

3DCRT	Three-Dimensional Conformal Radiation Therapy
ACH	Auckland City Hospital
BB (s)	Ball Bearing(s)
CCCS	Collapsed Cone Convolution Superposition
CPE	Charged Particle Equilibrium
CRT	Conformal Radiation Therapy
CT	Computed tomography
CTV	Clinical tumour volume
DNA	Deoxyribose nucleic acid
DVH	Dose volume histogram
EBRT	External beam radiation therapy
EUD	Equivalent uniform dose
GTV	Gross tumour volume
Gy	Gray (J/kg)
IAEA	International Atomic Energy Agency
ICRU	International Commission on Radiation Units and measurements
IMRT	Intensity-modulated radiation therapy
KERMA	Kinetic Energy Released in the Medium
MLC	Multi-leaf collimator
MOSFET	Metal Oxide Semiconductor Field Effect Transistor
MU(s)	Monitor unit (s)
MV	Mega-voltage
netOD	Net Optical Density
OAR (s)	Organ(s) at risk
OD	Optical Density
PAS	Plan Assessment Sheet
PTV	Planning target volume
QUANTEC	Quantitative Analysis of Normal Tissue Effects in the Clinic
ROI (s)	Region(s) of interest
RT	Radiation therapy

SAD	Surface-to-axis distance
SSD	Source-to-surface distance
SSDL	Secondary Standards Dosimetry Laboratory
TCPE	Transient Charged Particle Equilibrium
TERMA	Total Energy Released per unit Mass
TIFF	Tagged image file format
TLD	Thermoluminescent detector
TPS	Treatment planning system
TRS	Technical Reports Series
VMAT	Volumetric modulated arc therapy

1. Introduction

The uncontrolled growth of abnormal cells anywhere in the body is termed cancer. Radiotherapy, surgery and chemotherapy are the most common treatments for cancer - surgery and radiotherapy are used to treat localised tumours whilst chemotherapy is used to treat cancers which have spread. More than half of all patients treated for cancer, at some stage, will require radiotherapy [1, 2].

This thesis details work carried out to establish whether bolus material is necessary to ensure that the scars on the skin of head and neck radiotherapy patients receive a full dose of radiation. A planning study was performed to investigate whether full dose to the skin could be achieved without bolus via the usual planning process, as well as a range of other advanced planning techniques. The results of this study were verified with a phantom study and film dosimetry.

The thesis begins with an overview of external beam radiotherapy including important radiation-tissue interactions which ultimately lead to cell kill in tumours in section 1.1.1. A brief description of a linear accelerator is given in section 1.1.2. Section 1.1.3 explains the skin sparing effect of high energy photon beams. Section 1.1.4 introduces the various radiotherapy treatment techniques that may be used to treat head and neck cancer. Section 1.1.5 gives a brief description of external beam radiotherapy for head and neck cancer and section 1.2 gives an overview of the treatment planning system. The dosimetry equipment and materials best suited for measuring surface dose are discussed in section 1.3. Section 1.4 gives an overview of bolus. Finally, the objective of this thesis is given in section 1.5.

1.1 External Beam Radiation Therapy

1.1.1 Radiobiology

External beam radiation therapy (EBRT) is a treatment modality which relies on the destruction of tumour cells by irradiating them with a beam of ionising radiation. When ionising radiation travels through matter, it loses energy through a variety of

processes (discussed in section 1.1.3) which result in the ionisation of local atoms. When the material is tissue, the ionisation events in a cell can damage the cell's DNA by direct or indirect action. In direct action, single or double DNA strands are broken. This may lead to irreversible cell damage. In indirect action the ionising radiation interacts with other molecules or atoms in the cell producing free radicals. The highly reactive free radicals produce changes that cause biological damage. If the cell cannot repair itself correctly it will either become inactive or will undergo programmed cell death. More radiation damage means less likelihood of cell repair and thus a higher chance of cell death. The aim of EBRT is to cause maximum damage to the tumour while minimising damage to non-tumorous tissues surrounding it [3].

1.1.2 Linear Accelerators

In the early days of radiotherapy only superficial disease could be treated as the only available therapeutic beams were low energy X-rays which had a limited penetration depth. The desire to treat tumours at greater depths required the use of higher energy beams and this led to the development of Cobalt-60 machines and subsequently to the development of the modern linear accelerator [4].

Linear accelerators are machines which produce high energy photons and electron beams for radiation treatment. Modern linear accelerators have the ability to produce multiple electron and photon energies and they can deliver radiation doses at high dose rates. The linear accelerator uses microwave technology to accelerate electrons in part of accelerator called the 'wave guide'. These accelerated electrons are then allowed to collide with a heavy metal target to produce a high energy photon beam (Fig. 1.1). The beam of high energy photons is shaped as it exits the machine to conform to the shape of the tumour. The shape of the photon beam is defined by collimator jaws and multileaf collimators (MLCs) made up of a high atomic number material. MLCs are made of two banks of interlocking tungsten leaves. MLCs have 40-120 leaves and each leaf can be moved individually to form an arbitrarily shaped field. The amount of radiation exiting the linear accelerator is measured in terms of monitor units (MUs) [5].

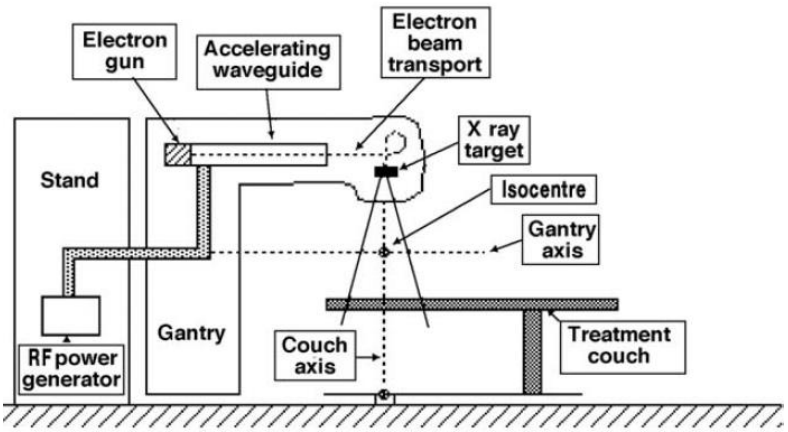

Figure 1.1: Schematic diagram of linear accelerator [5]**.**

In order to irradiate the tumour from a variety of angles, the gantry can be rotated around the patient lying on the treatment couch (Fig.1.2). During treatment delivery the patient position must replicate the planning computer tomography (CT) position to ensure that the radiation dose is delivered to the tumour. Hence, external markers are drawn on the patient's skin at the time of CT scan and the patient is then positioned on the treatment couch by aligning the external markers with the orthogonal lasers in the treatment room [5, 6].

Figure 1.2: Gantry rotates around the patient to irradiate the tumour from different angles [7]**.**

1.1.3 Photon interactions with matter

When a photon beam of energy hv travels through a medium (for example, tissue), it loses energy to the surrounding medium. When a photon interacts with an electron (assumed at rest), a part or all of its energy is converted into kinetic energy of the electron. In the case of partial energy transfer, the photon itself is scattered with decreased energy hv' (Fig. 1.3). The scattered photon may interact with electrons

resulting in partial or complete transfer of energy. The initial energy transferred from the photons to electrons is called collision KERMA (Kinetic Energy Released in the Medium) [8].

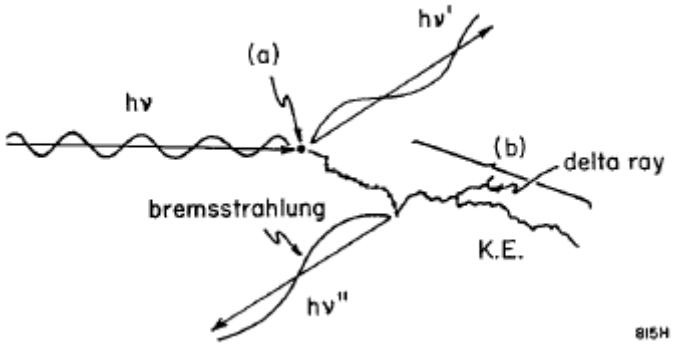

Figure 1.3: Schematic diagram of energy transfer from a photon to the surrounding medium. KERMA occurs at one point in the medium (a) but absorbed dose occurs further downstream and over a path length (b) [8].

After receiving energy the electron traverses through the medium and loses its energy in collisions along its path (indicated by (b) in Fig. 1.3). The energy transferred along its path is called the absorbed dose. Along its path the electron may collide with a nucleus resulting in a bremsstrahlung photon hν" ('bremsstrahlung loss'). This interaction is called radiative KERMA. An electron-electron collision may occur resulting in a delta ray. Both KERMA and absorbed dose have the same unit: joules/kg [8, 9].

As the photon fluence is greatest at the surface, the initial energy transfer from photon to electron (collision KERMA) is highest at the surface. On the other hand, absorbed dose (energy transferred by the electron along its path to the medium) is lowest at the surface (as electronic equilibrium has not yet been reached – see below) and increases with depth. It reaches a maximum value at z_{max}. If there was no photon attenuation or scattering in the medium, KERMA would be constant with depth. The region between the surface and z_{max} is called the build-up region. If the bremsstrahlung losses were ignored, the absorbed dose would be equal to KERMA beyond z_{max}. This would result in a region of charged particle equilibrium (CPE) (Fig.1.4) [8, 9, 10].

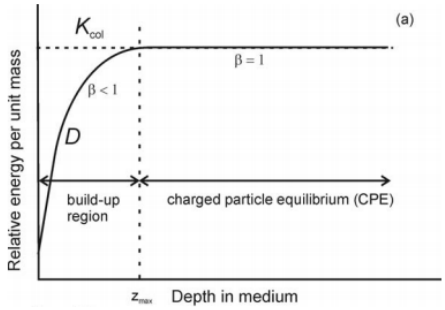

Figure 1.4 : In the absence of attenuation and scattering, the number of electrons released per unit length remains constant and CPE is achieved [9] .

However, in practice, the photons are attenuated and scattered in the medium and the number of secondary electrons also decreases. So both KERMA and absorbed dose decrease. In this case the region beyond z_{max} is called transient charged particle equilibrium (TCPE) (Fig. 1.5) [8, 9, 10].

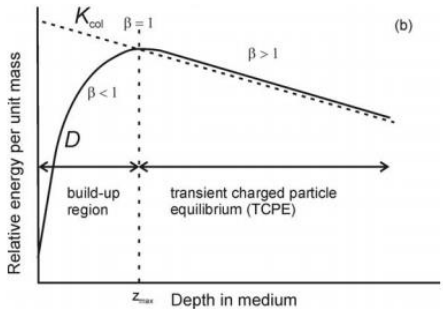

Figure 1.5: Number of electrons released per unit length decreases due to photon attenuation and scattering in the medium resulting in TCPE [9].

Therefore the absorbed dose at the surface is smaller than the dose at $z_{max.}$ This is called the skin sparing effect of high energy photon beams. It allows the optimal doses to be delivered to a deep seated tumour without causing severe skin reactions. The skin sparing effect increases as photon energy is increased [5].

1.1.4 Conformal Radiation Therapy

Before the advent of modern technology, radiation treatments were based on orthogonal X-ray images and dose was calculated manually. The beam arrangement was usually coplanar, with two to four opposing beams. [11, 12]. With the introduction of CT images and computerised treatment planning systems, it became possible to plan three-dimensional conformal radiotherapy (3DCRT). Multiple beams from different angles were directed to the tumour such that the high dose volume conformed to the shape of the target volume whilst sparing the normal tissues [13].

Its limitation was that a large number of beams is required to achieve an optimal dose distribution for complex-shaped tumours [14].

1.1.4.1 Target Volumes

It is important to define the target volume on the CT images for the purpose of planning the treatment. The International Commission on Radiation Units and Measures (ICRU) reports 50, 62, and 83 provide the foundations to define the target volumes. The three main volumes are the gross tumour volume (GTV) i.e. the tumour visible on planning images, the clinical target volume (CTV) and the planning target volume (PTV) (Fig. 1.6). The CTV comprises the GTV plus a margin for microscopic spread. The CTV must be adequately treated to cure the disease. The PTV incorporates the CTV plus margins to account for possible uncertainties in patient positioning, organ motion, and beam alignment. Dose is prescribed to the PTV to ensure that the CTV receives an adequate dose. As per ICRU recommendations, at least 95% of the prescribed dose should be delivered to the PTV to deliver full dose to the CTV [15, 16].

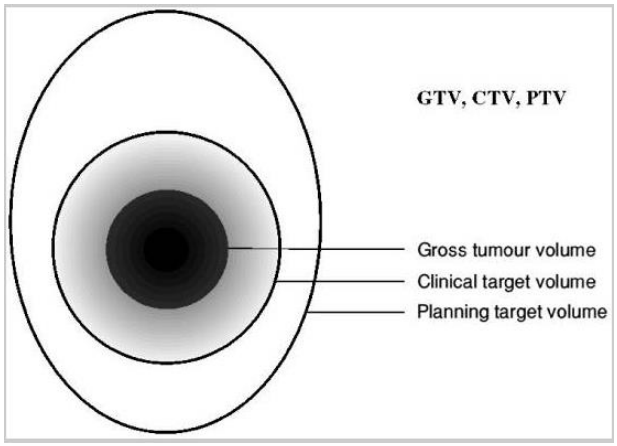

Figure 1.6: Main target volumes in radiotherapy [15].

1.1.4.2 Intensity Modulated Radiation Therapy

Intensity Modulated Radiation Therapy (IMRT) is an advanced form of CRT in which the intensity profile of at least one beam is modulated. The beam intensities can be modulated using MLCs. Each beam is divided into several beamlets and each beamlet has a fixed intensity. This allows conformation to complex shapes, even those with concavities, such as that shown in Fig. 1.7. The superposition of

independent segmented fields delivered from different gantry angles produces the desired dose distribution, and limit dose to organs at risk [17]. IMRT plans are generated using inverse planning techniques. The inverse planning technique uses a mathematical optimization algorithm to generate a deliverable treatment plan that produces a dose distribution closest to the prescribed one [18].

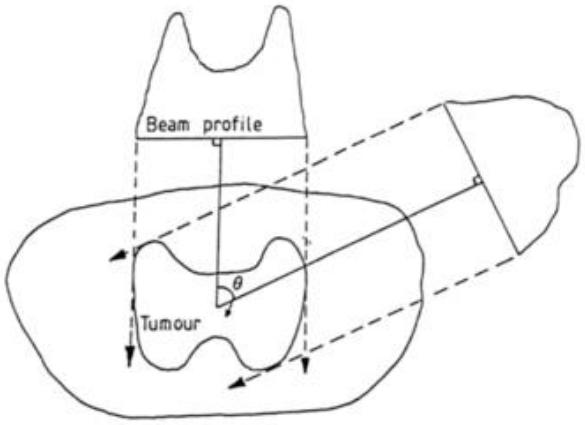

Figure 1.7: Intensity modulated beams. The beams superimpose to deliver high dose to the tumour whilst sparing the surrounding normal tissues [19].

The optimization criteria are commonly expressed in terms of dose objectives and weightings. The treatment planner sets desired goals for target volumes and the organs at risk (OARs). For example, the planner may set minimum and maximum dose values for the PTV and give these parameters high weighting to produce a homogenous dose in the PTV. The planner can also apply a 'mean' or 'uniform' dose constraint for the PTV. The planner may assign a maximum dose for an OAR with lower weighting. The optimization function then will try to achieve these goals. The minimum and maximum dose values for the PTV are generally 95% and 105% respectively based on recommendations in ICRU 83. The maximum dose limits for different OARs are different and are based on the Quantitative Analysis of Normal Tissue Effects in the Clinic (QUANTEC) guidelines. The optimization criterion can also be defined in terms of an equivalent uniform dose (EUD). EUD is defined as the biologically equivalent dose which, if given uniformly, will result in killing the same number of cells in a specific organ as the actual non-uniform dose distribution [18].

The planner also determines the number of beams and beam angles considering the shape, size, and location of the target volume and gives this as an input to the

planning system. This is called 'beam angle optimization'. Based on the optimization criteria, the optimization algorithm then generates a fluence map for each beamlet in each beam ('fluence map optimization') and uses the leaf-sequencing algorithm to convert these fluence maps into a series of MLC shapes (segments). These segments are saved as an MLC leaf sequence file. The MLC leaf sequence file controls the movement of MLCs during treatment delivery [17, 20].

IMRT can be delivered by two methods – step-and-shoot and dynamic delivery. In step-and-shoot the photon beam switches off whilst the MLC leaves travel from one segment to another. The total dose at one point is the superposition of doses from each of the segments. On the other hand, in a dynamic delivery the MLC leaves move across the beam aperture at different speeds to 'paint' a continuous fluence map when the beam is on [17].

Many studies have shown that IMRT can increase locoregional control and reduce toxicity, thus reducing side effects and improving quality of life [11]. However, the treatment time required to deliver an IMRT treatment is greater compared to 3D CRT. This has led to newer advanced techniques which can deliver complex dose distributions in a shorter treatment time [21].

1.1.4.3 Volumetric Modulated Arc Therapy

Volumetric modulated arc therapy (VMAT) is a rotational form of fixed gantry IMRT. In VMAT, the MLC leaves move as the gantry rotates whilst the beam is on. Three parameters – gantry rotation speed, beam aperture shape and dose rate are varied simultaneously during the treatment delivery to produce a highly conformal dose distribution with a reduced treatment time and fewer MUs compared with IMRT [21].

In VMAT planning it is considered that the full arc (360° gantry rotation) can be represented by a number of control points. VMAT optimization starts with modelling the continuous gantry motion as the coarse sampling of static gantry positions. The fluence map at each gantry position is optimized and then converted into control points. Only two control points are selected and the rest are discarded. By

interpolating between the existing control points, new control points are added. Thus the gantry resolution is gradually increased until a desired control point density is reached (typically one control point at every 2°-4°). The machine constraints (gantry rotation speed, leaf translation speed, and maximum dose rate) are considered while optimizing these control points [22, 23]. Fig. 1.8 illustrates VMAT optimization.

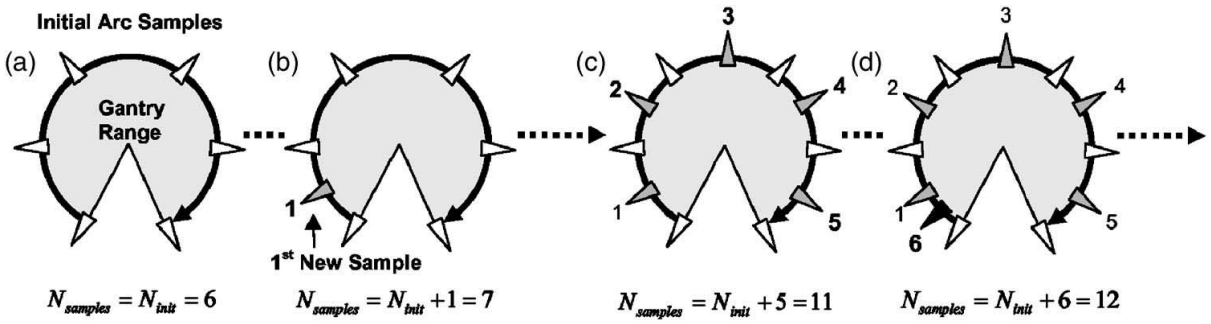

Figure 1.8: VMAT optimization process. The continuous gantry motion and MLC configuration is modelled as coarse sampling of static gantry positions. As the optimization continues more samples are added to get desired sampling frequency [22].

VMAT is considered to have an advantage over IMRT such as a having shorter delivery time and fewer MUs whilst maintaining a comparable dose distribution. However, VMAT treatment planning is more challenging than IMRT planning as it is necessary to process a large amount of data. Furthermore, VMAT plans are computed as a finite series of stationary fields but the delivery is continuous. The constraints placed on the speed of MLC leaf translation between successive gantry angles can affect the delivery of the plan. All these factors must be considered whilst developing a VMAT plan and the plan must be delivered and verified on the linear accelerator before treatment delivery [23].

1.1.5 EBRT for Head and Neck cancer

Head and neck cancer is a broad term that covers epithelial malignancies that occur in the paranasal sinuses, nasal cavity, oral cavity, pharynx, and larynx. Most commonly these are squamous cell carcinomas of the head and neck [24].

For some sites, such as tongue cancer, surgical removal of the tumour may be curative. If the tumour is non-resectable or if there is a risk that the surgery may give a poor cosmetic or functional outcome, radiation therapy is the main treatment

modality. It is also used as adjuvant therapy to treat the postsurgical bed of primary tumours and/or adjacent areas where the tumour may have infiltrated [1].

The geometry of the target volume in head and neck cancer is often complex. The complexity of the treatment increases due to the close proximity of many physiologically important OARs (for example, the optic nerve) near the target. Often the distance between the target volume and OARs is not greater than a few millimetres. Therefore the goal of the treatment is not only to treat the tumour but also to maintain the functionality of the OARs. It can be difficult to deliver the required dose to the target volume whilst minimising dose to critical structures using conventional 3DCRT. Hence advanced conformal radiation therapy such as IMRT and VMAT are used (Fig. 1.9) [24, 25, 26].

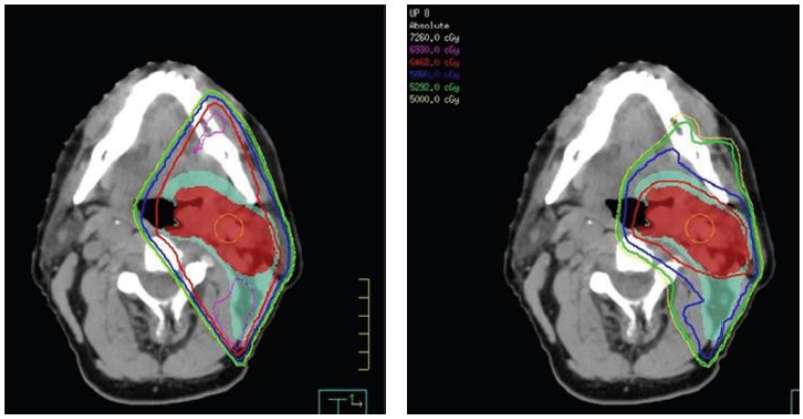

Figure 1.9: Comparison between a conventional 3DCRT and IMRT plan. a) In the 3DCRT plan the 98% isodose line (red line) covers the high risk target volume (red ROI) as well as the low risk target volume (green ROI) and surrounding critical organs. b) In the IMRT plan the 98% isodose line conforms to the high dose region more tightly [26].

1.2 Treatment Planning System

The computerised treatment planning system (TPS) plays a central role in EBRT. The TPS provides tools for the radiation oncologists, radiation therapists and medical physicists to generate beam shapes and dose distributions to achieve the treatment goals. During the commissioning process of a TPS, various radiation beam parameters (for example, central axis depth dose, beam profile etc.) are fed into the TPS to model the treatment beam. The TPS uses CT data sets to generate 3D models

of the patient's anatomy and tumour targets. The radiation oncologist contours the target volumes and organs at risk (OARs) on the images. A virtual patient is created to generate a simulation of the treatment plan using the beam model and patient data [5].

The treatment plans are evaluated by analysing the dose distribution. The treatment plans are verified to ensure that the PTV is covered adequately and doses to OARs surrounding the PTV are low enough not to induce significant toxicity. The most commonly used tools for dose distribution analysis are isodose curves, dose distribution statistics and dose volume histograms (DVH). The isodose curves show the spatial distribution of dose superimposed on the CT images. Dose distribution statistics give quantitative information on the dose received by the PTV or OARs, such as minimum dose to the volume (D_{min}), maximum dose to the volume (D_{max}), and mean dose to the volume (D_{mean}). The statistical characteristics also include dose-volume parameters such as D_v and V_D. D_v is the absorbed dose that covers a specified volume (V) of the target. For example, $D_{50\%}$ means the dose received by at least 50% of the volume. On the other hand, V_D is the percentage of volume that receives the prescribed dose (D). For example, $V_{95\%}$ is the percentage of volume receiving 95% of the prescribed dose. DVHs provide the summary of a 3D dose distribution within a structure displayed as a 1D curve. It is a useful tool to compare various treatment plans from different planning techniques. There are two types of DVH - differential DVH and cumulative DVH. The cumulative DVH is most commonly used for treatment plan evaluation. A cumulative DVH shows the fraction/percentage of volume that receives at least a dose D. An example of a cumulative DVH is given in Fig.1.10 [5].

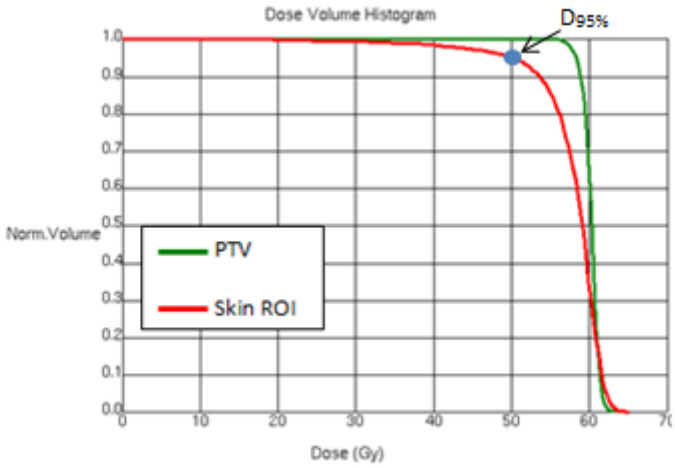

Figure 1.10: Cumulative DVH. The fraction of volume receiving at least a dose D is plotted against dose. For example, $D_{95\%}$ (indicated by blue dot) for the skin ROI is 50 Gy. In other words, 95% of the skin ROI volume receives at least 50 Gy.

All plans in this study were developed using Pinnacle[3] treatment planning system (Phillips Medical Systems, Andover, MA).

1.2.1 Pinnacle [3]

Treatment planning in Pinnacle[3] starts with the contouring of different regions of interest (ROIs). In addition to PTVs and OARs, extra planning ROIs are needed to allow rapid dose fall off outside of the PTV as well as to avoid high doses to critical structures. For example, a 'ring' ROI of 0.3 mm is created around PTV to create a sharp dose gradient outside PTV [27].

The following flow chart explains the IMRT and VMAT treatment planning process.

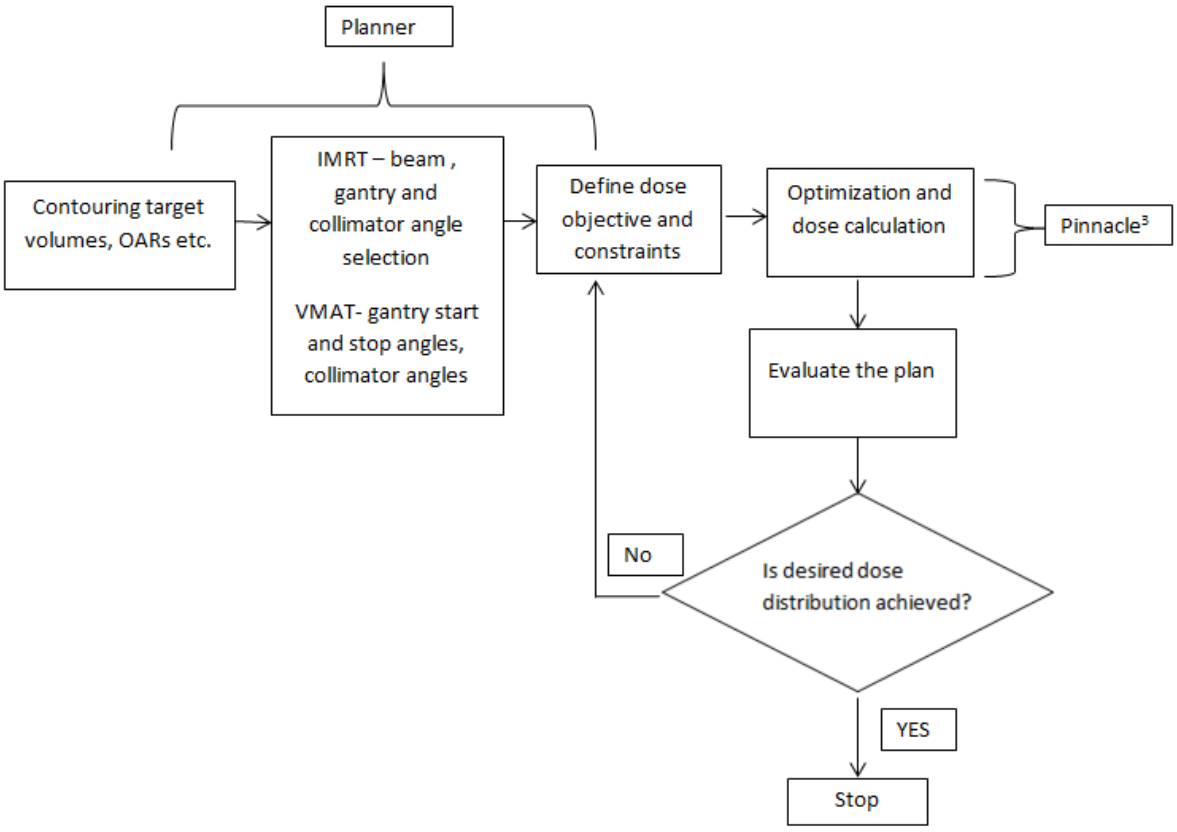

Figure 1.11: Flow chart for IMRT and VMAT treatment planning.

The dose distribution in Pinnacle[3] is calculated using the Collapsed Cone Convolution Superposition (CCCS) algorithm. In this algorithm, the incident energy fluence plane is projected through the CT patient representation and is attenuated using the mass attenuation coefficient to calculate the total energy released per unit mass (TERMA). The secondary electrons which receive TERMA travel away from the point where the initial energy was released. As they travel they deposit energy along their path. The energy deposition kernel accounts for the dose deposited at a point (r) from energy released at a different point (r') (Fig.1.12) [18, 28] .

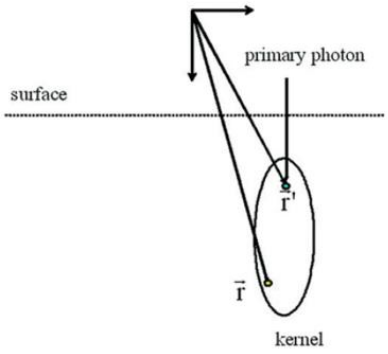

Figure 1.12: The dose deposition kernel. The energy deposition kernel accounts for the dose deposited at a point (r) from energy released at a different point (r') [18].

Three dimensional dose distributions are calculated by superposing the TERMA with the energy deposition kernel at that specific voxel. The doses from multiple beams are calculated separately and finally added together as per the corresponding beam weight [28].

When megavoltage photons pass through the linear accelerator, they interact with various components in the head (such as the collimation system) resulting in the production of contamination electrons. These contamination electrons contribute to the surface dose. Electron contamination modelling in Pinnacle^3 is simplified by assuming that the electron contamination does not depend on the source-to-surface distance or on other beam modifiers. It is modelled as an exponential fall off and is added to the overall dose. This can lead to significant discrepancies between the surface dose calculated by Pinnacle^3 and the actual delivered surface dose [29, 30].

1.3 Dosimetry

Radiation detectors play an important role in ensuring the correct delivery of the treatment plan. Radiation detectors are regularly used for quality assurance of the machine as well as the verification of the treatment plans. There are many different types of radiation detectors such as ionization chambers, radiochromic films, thermoluminescent detectors (TLD) etc [5, 31]. In this study, ionization chamber and radiochromic film are used for dose measurements.

1.3.1 Ionization chambers

A cylindrical ionization chamber is an air filled cavity which is surrounded by a conductive outer wall and has a central collecting electrode. The wall and the collecting electrode are separated with a high quality insulator to minimize the leakage current when a polarizing voltage is applied to the chamber. The cylindrical ionization chambers have a typical volume between 0.04-1.00 cm^3 (Fig 1.13 a). They are generally used for calibrating radiation beams as well as point dose measurements in plan verification. An electrometer is used to measure the generated signal [5].

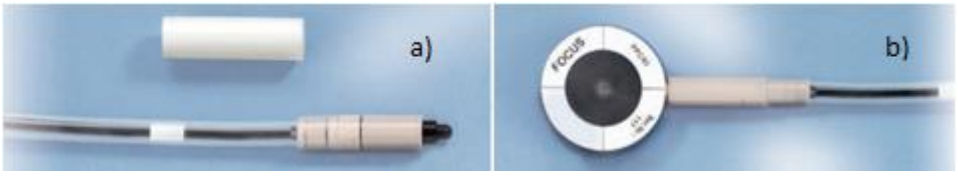

Figure 1.13: a) 0.04 cc cylindrical ionisation chamber. b) PPC40 parallel plate ionization chamber [32]

Another type of ionization chamber is the parallel-plate ionization chamber (Fig. 1.13 b). The parallel-plate ionization chamber consists of two parallel plate electrodes which are separated by a fixed distance (~2 mm). The entry window is a polarizing electrode and the back wall is a measuring or collecting electrode. The guard ring surrounds the collecting electrode. It is insulated from the collector but is kept at the same potential to minimize the charge leakage [5, 33]. In photon beam dosimetry, the parallel plate chamber is used to measure the surface dose and depth dose measurements in the build-up region as they have a thin entrance window and good spatial resolution in the z-direction. However, these chambers show over-response in the build-up region to some degree based on their internal dimensions. The main source of the over-response is secondary electrons scattering from the side wall of the chamber. Gerbi's correction factors can be applied to correct the over- response. These factors are based on guard size, plate separation, and volume of the parallel plate chamber and are specific to each chamber design [34, 35, 36].

The calibration factors for ionization chambers can be obtained by either calibrating them at a secondary standards dosimetry laboratory (SSDL) or through cross-calibration with another ionization chamber calibrated at SSDL using standard

protocols such as IAEA-TRS 398 [5]. The calibration factor is used to convert the chamber reading into absorbed dose. If the experimental conditions are different from the reference conditions at the time of calibration, corrections factors are applied [5]. The list of correction factors is given in Appendix A.

When an ionization chamber is placed in a high energy photon beam, it introduces a displacement effect. The displacement effect is the perturbation of the measured signal, caused by the displacement of the surrounding medium by the detector. It depends upon the spatial dimensions of the detector. The preferred and most commonly used method for correcting this is the effective point of measurement. In this method, the volume averaged ionization within the ionization chamber is not reported to the chamber's reference point but to a point within the air filled cavity [37]. For a parallel plate chamber, it is defined at the inside surface of its front window. This point is positioned at the desired depth of measurement (Fig. 1.14) [38].

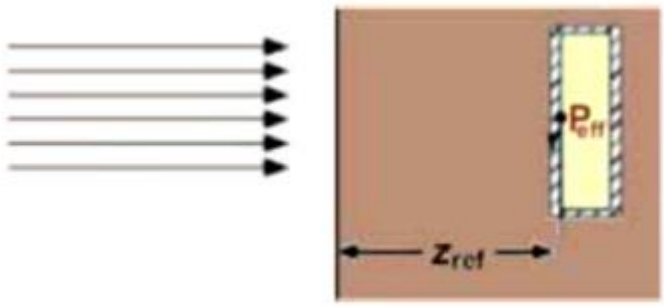

Figure 1.14: Effective point of measurement for a parallel plate chamber [39].

1.3.2 Radiochromic film

While parallel plate chambers can be used for central axis depth dose measurements in the build-up region either in water or in a solid water slab phantom, their significant size makes it impossible to use them for measuring surface dose on a patient or anthropomorphic phantom. For this purpose radiochromic films are suitable, since they are extremely thin. [36].

Radiochromic films are insensitive to visible light. They contain a special radio-sensitive dye in the form of microcrystals, which are embedded in a gelatin binder.

When the film is exposed to ionizing radiation the microcrystals polymerize and change the colour of the film to blue. The amount of polymerization and degree of colour change is proportional to the absorbed dose (Fig 1.15). The polymers absorb light and the transmission of light through the film can be measured with a suitable densitometer such as flatbed colour scanner [40].

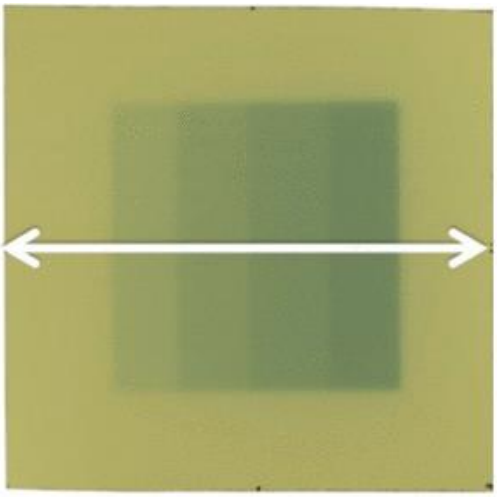

Figure 1.15: EBT3 film response to different dose levels (0.6, 1.1,1.6, and 2 Gy) . As the dose increases the film becomes darker [41]**.**

To find out the radiation dose delivered to the film, the change in optical density of the film is measured (Fig. 1.16). The optical density (OD) is defined as

$$\mathrm{OD} = -\log_{10}\left(\frac{\mathrm{I}}{\mathrm{I}_0}\right) \quad \text{Eq. 1}$$

where I_0 = initial intensity, I = transmitted intensity [40]

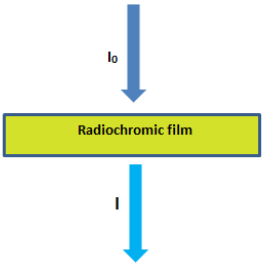

Figure 1.16: I_0 is the intensity of incident light and I is the intensity of light transmitted through the film.

The OD measured is dependent on the wavelength of light used for analysis, the emission spectrum of the light source and spectral sensitivity of the light detector. To determine the relationship between absorbed dose and film response, a calibration curve is used. A range of known doses, which includes the dose of interest, is delivered to the film and the change in OD is measured to obtain the

calibration curve. The relationship between dose and OD is not linear. Hence different methods, such as polynomial fits, are used to describe the relationship [40] (Fig 1.17).

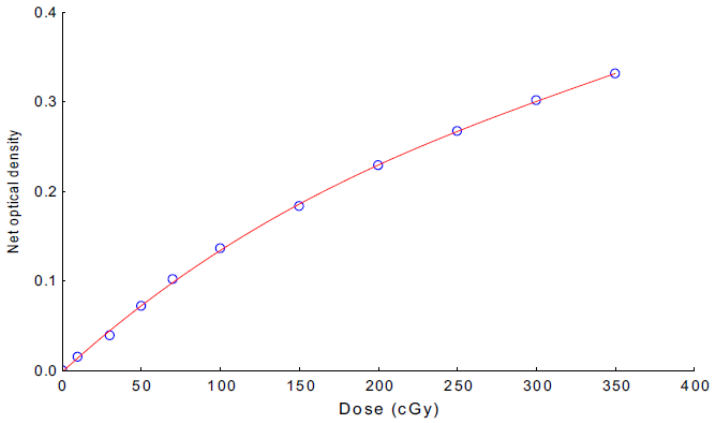

Figure 1.17: A typical EBT3 film calibration curve. The relationship between dose and optical density is not linear [42].

1.3.2.1 Gafchromic EBT3

Gafchromic® dosimetry films are the most commonly used radiochromic films. The latest Gafchromic film introduced in the market is EBT3. Like the previous EBT models, EBT3 contains lithium salt of pentacosa-10, 12-diynoate (LiPAD) as the active component [43]. It has a single 28 µm thick active layer consisting of the active component, maker dye, and stabilizers. The yellow marker dye is used for uniformity corrections. The active layer is sandwiched between two transparent 100 µm thick polyester substrate layers (Fig. 1.18). This eliminates the face-up/down orientation effect as it generates identical scans. The polyester layers are laminated with silica particles to induce a 5 µm gap between the scanner surface and film. As the gap is almost ten times the wavelength of visible light, the Newton Ring artifact in images is avoided [44, 45].

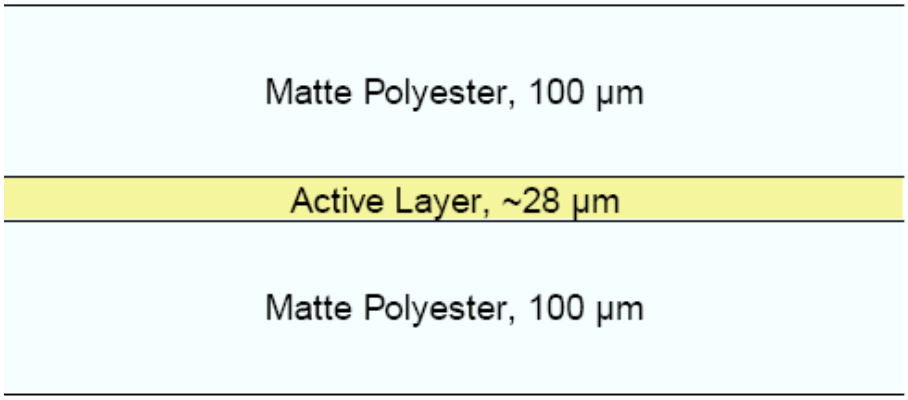

Figure 1.18: Configuration of GafChromic EBT3 film [45].

1.3.2.2 Advantages of EBT3 films

All models of Gafchromic EBT films are self-developing. They have a water-equivalent atomic number, and are suitable for use in the clinical dose range (0.1-10 Gy). Since they are relatively insensitive to visible light, film handling has become easier. They are energy- independent for a wide range of energies (25 MeV to 384 keV) [46]. Their response to ionizing radiation is independent of dose rate, at dose rates from 0.08 to 80 Gy/min. They are thin and can be cut to the desired size and shape. They have high spatial resolution and low spectral sensitivity which makes them ideal for measurements in steep dose gradient. The other advantage of radiochromic films over other dosimeters is that it is a 2D dosimeter. While other dosimeters (for example, ionization chamber) measure point doses, film can measure dose to the region of interest [47]. The previous Gafchromic EBT models (EBT and EBT2) suffered from Newton ring artefact. EBT3 films have a polyester film substrate with silica treatment which prevents the ring formation [43].

1.3.2.3 Limitations of EBT3 films

Radiochromic films do not give instant readouts. Even though post processing is not required, the response of the film must be converted into absorbed dose using the previously discussed calibration curve. For good reproducibility and reliable results, strict scanning protocols must be followed. As there is batch-to-batch variation in films, the calibration curve should be obtained for each batch. The active monomer (LiPAD) has a hair-like structure and after polymerization they tend to align with each other. This causes anisotropic light scattering. This means that the orientation of film during scanning affects the measured OD. Thus the film responses in

landscape and portrait orientation are different. If the films are scanned in landscape orientation during calibration, the films must be scanned in landscape direction for other measurements too. Otherwise it will introduce a significant error in measurement. Hence it is recommended to maintain the same orientation for all measurements. The films should always be placed in the central area of scanner to ensure that the non-uniformity of scanner does not affect the reading. The film continues to darken over time after irradiation. Therefore there should be a minimum 20-24 hours period between exposure and scanning. The film response can vary with temperature [40, 44] .

1.4 Bolus

As discussed in section 1.1.3, megavoltage photon beams have skin-sparing effect. Hence, to treat superficial lesions, such as scar tissues in postoperative radiotherapy for head and neck cancer, a bolus is used to provide adequate absorbed dose to the surficial lesions. As the purpose of using bolus is to introduce additional tissue in the path of the beam at patient's surface, the bolus material should be tissue-equivalent. Commonly used bolus materials are paraffin wax, cotton soaked with water, rubber, and jelly-like material [48]. At Auckland City Hospital, a jelly-like material with a physical density of 1.0 g/cm^3 is used as bolus for head and neck cancer. Its thickness is 7 mm. The radiation oncologist draws the outline of area to be treated on the patient's skin. A tracing of this outline is used to make the bolus. During the treatment, the bolus is placed on the region of interest. It is custom-made for each patient.

1.5 Objectives

EBRT is used as adjuvant therapy to treat the postsurgical bed of primary tumours and regional lymph nodes in head and neck cancer treatment. Hence bolus is used to provide dose build-up and deliver high doses to scar tissue on skin [1]. However, considerable time and resources are required to make bolus.

Studies have shown that the use of tangential beams, immobilization masks and including skin in the target volume in IMRT and VMAT plans can result in higher surface doses [49, 50, 51]. Chow and colleagues measured the surface dose with a metal oxide semiconductor field effect transistor (MOSFET) detector and found that for a prostate patient the surface dose in IMRT plans was 15% to 30% higher depending upon the number of beams [52]. Higgins *et al* [53] investigated the difference between the surface dose in conventional radiotherapy with open fields and IMRT plan for a head and neck case study. Their study showed that the surface dose increased by 13% when IMRT technique was used.

This study aims to find out whether IMRT and VMAT plans for post-operative head and neck cancer patients can be developed ***without bolus*** to achieve the same treatment goals as those ***with bolus***, by comparing the 95% isodose coverage of the planning target volume (PTV) as well as the surface dose delivered by different treatment plans. The surface dose will be verified using radiochromic EBT3 film dosimetry.

2. Materials and Methods

This chapter includes the data collection and analysis techniques as well as the materials used in this study. The patient selection method is described in section 2.1. The subsequent sections include the various aspects of treatment planning, including contouring ROIs, planning objectives and treatment planning techniques. Section 2.3 describes the dosimetry study. It talks about the different aspects of radiochromic film dosimetry and the comparison between surface doses measured with film and parallel plate chamber measurement. The surface doses in the original plans with bolus and new no bolus plans were verified by delivering the treatment plans to a phantom and measuring the surface dose with film. The details of the surface dose verification are given in section 2.3.5.

2.1 Patient Selection

For this retrospective study, ten patient plans were randomly selected from the list of patients who had received adjuvant post-operative IMRT for head and neck cancer at the Radiation Oncology Department of Auckland City Hospital (ACH). The patient plans were developed using Pinnacle^{3}® Radiation Therapy Planning software (Philips Medical Systems). All patients were scanned with bolus already positioned on scar tissue on the skin. Bolus was used to increase the dose to post-surgical scar tissues.

2.2 Treatment Planning Study

The goal of the treatment planning study was to investigate whether it was possible to generate a clinically acceptable plan ***without bolus*** that would maintain a 95% isodose coverage of the planning target volumes (PTVs) whilst also delivering adequate dose to scar tissues on the skin. The clinical acceptability of the plan was determined by comparing the PTV coverage and organ at risk doses in the new plan with those in the original plan. A range of treatment planning techniques such as IMRT, 1 full arc VMAT, 2 full arcs VMAT and two-partial arcs VMAT were used to create the new ‘no bolus’ plans. These techniques are commonly used for head and neck treatment planning. An in-house script developed for plan assessment was

used to obtain the dose statistics for PTV, OARs and the skin ROI dose. Using this script, the DVH data of region of interest (both targets and OARs) are exported from Pinnacle[3] and read into an in-house spreadsheet which calculates the dose statistics for that region (D_v or V_D). An example of the plan assessment sheet (PAS) is given in Appendix B.

2.2.1 Contouring

The planning CT scan for each patient was prepared for the planning study by generating the following contours: The bolus was carefully outlined on each slice and then a skin region of interest (ROI) was added. The skin ROI was a 5 mm thick volume drawn under the bolus (Fig 2.1). The 5 mm thickness was chosen to include three layers of the skin (epidermis, dermis, and hypodermis) [54, 55].

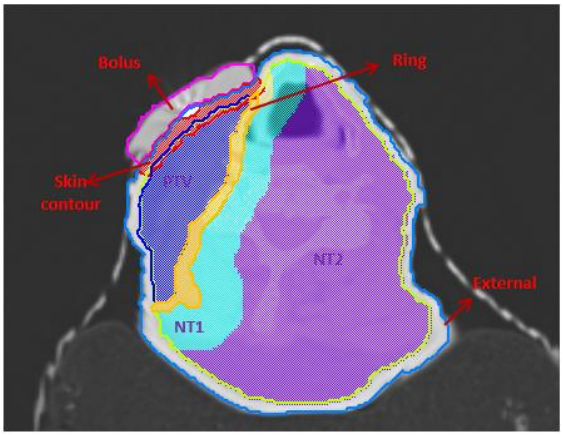

Figure 2.1: Regions of interest (ROIs). Two new ROIs- Bolus and Skin- were added to the original plan and other ROIs were edited to aid the optimisation process.

In order to evaluate the effect of removing the bolus, it was necessary to cut the bolus from the external patient contour. The original plans were first copied and in the new copied plans the physical density of bolus was overridden, i.e. set to zero (density of air). A 3 mm strip of tissue closest to the patient's surface was removed from PTVs and other ROIs for optimization purpose since the optimization algorithm needs to work very hard to achieve full dose here and this can result in hotspots in other parts of the plan.

2.2.2 Dose objectives

The 'no bolus' planning study was divided into two parts- 1) PTV coverage optimization 2) Skin dose optimization. ICRU states that the PTV should be covered at least with 95% of prescribed dose in order to deliver adequate dose to the CTV [56]. Hence, in PTV coverage optimization, the goal was to get an optimal 95% isodose coverage of PTV and observe its effect on the skin dose. On the other hand, in 'Skin dose optimization', the plans were optimized to maintain full dose to the skin ROI and observe its effect on the rest of the plan.

2.2.2.1. PTV coverage optimization

In order to generate a new treatment plan without bolus, the dose objectives were initially set using departmental guidelines. Table 2.1 describes tried and tested parameters which help to give the optimiser a starting point to produce an acceptable treatment plan. The target dose objectives were then adjusted to produce a dose distribution which matched the original bolus plans as closely as possible. Following this, an assessment of the impact of missing bolus on skin dose was performed.

Table 2.1: Optimization objective types in Pinnacle[3]

Objective type	Description
Max Dose	sets the desired maximum dose in an ROI; when used for PTV usually set at 105 % of the prescribed dose; usually set with a low weight in PTVs (when combined with the Min Dose and Uniform Dose objective); when used for OARs usually set at maximum dose limit for that organ.
Min Dose	sets the desired minimum dose in an ROI; used only in PTVs and usually set at 95% of the PTV's dose prescription (e.g. 57Gy for PTV60); provides an additional control of the PTV coverage when used together with the Uniform Dose objective;
Uniform Dose	sets the desired uniform dose in an ROI; must only be used in PTVs and given the same (or comparable) weight as that of the Min Dose;
Max EUD and Min EUD	used to control hotspots, cold spots or the mean dose in an ROI; requires a parameter "a" where: i. a < 1 is appropriate for ROIs representing targets. A smaller (or more negative) "a-value" can remove cold spots; used with Min EUD ii. a = 1 corresponds to the mean dose; used with Max EUD iii. a > 1 is appropriate for ROIs representing critical structures. A larger "a-value" can remove hot spots; used with Max EUD

2.2.2.2 Skin dose optimization

To replicate the dose delivered in the original bolus plans, the percentage of prescribed dose to the skin ROI in the original plan was calculated for each patient using the formula

$$\%\ of\ prescribed\ dose\ received\ by\ skin = \frac{Mean\ dose\ to\ skin}{Prescription\ dose} \times 100 \qquad \text{Eq. 2}$$

It was found that, on average, 97.2% of the prescribed dose was delivered to the skin ROI in the original plans. Hence two patients were selected for whom the skin dose was close to this average value. For these two patients, separate plans were generated in order to maintain this dose to the skin ROI so that the effect on the rest of the plan could be investigated. For example, if the prescribed dose was 70 Gy, then the dose to the skin ROI was optimised to 68 Gy.

While optimizing the plans, the skin ROI was considered as a 'cold spot'. Cold spots are volumes of tissue that receive doses less than prescribed dose [57]. At ACH, a combination of two dose objectives, minimum dose and minimum EUD, is used to remove cold spots. Hence, these objectives were used to deliver full doses to the skin ROI.

2.2.3 IMRT

The selected plans were originally developed using Pinnacle^3 version 9.2. However, during the planning study, Pinnacle^3 was upgraded to version 9.8. Hence the original bolus plans were re-computed using version 9.8. Since the beam model was unchanged, there was no difference in the optimization. All no bolus plans were generated using version 9.8.

Step and shoot IMRT was used to generate no bolus plans with 6 MV energy and a dose rate of 300 MU/min. The number of beams varied according to the size and shape of the PTVs. The maximum number of segments was set to 80, 90 or 100 depending upon the size and shape of PTV as well as the number of beams used. The minimum segment area was set to 5 cm^2 and the minimum MUs per segment was set to 5 to ensure that the delivered treatment would match the planned treatment.

The final dose was calculated using the 'Collapsed Cone Convolution' (CCC) dose engine and a 0.250 cm dose grid.

2.2.4 VMAT

All VMAT plans were developed using Pinnacle[3] version 9.8. The gantry start and gantry stop angles were set as shown in Table 2.2 depending on the number of arcs used in the plan. The collimators were rotated to reduce the tongue and grove effect as well as dose to interleaf leakage. The gantry spacing was 4° and the maximum delivery time was set to 90 sec. The dose rate was 600 MU/min.

Table 2.2: Gantry and collimator settings for VMAT plans

	Gantry Start	Gantry Stop	Direction of Rotation	Collimator Angle
1 Full Arc	179°	181°	Counter-clock wise (CCW)	10°
2 Full Arcs				
Arc1	179°	181°	CCW	10°
Arc2	181°	179°	Clockwise	350°

The two-partial arc VMAT plans had one partial counter clockwise arc and one partial clockwise arc. The gantry start and stop angle were decided according to the position and shape of the PTV. The collimator angles for counter clockwise and clockwise arcs were 10° and 350° respectively.

2.3 Film Dosimetry

Film dosimetry was performed to verify whether the measured surface dose was in good agreement with the planned dose.

2.3.1 Film calibration

GafChromic EBT3 films (International Specialty Products, Wayne, NJ, USA) were used for film dosimetry. For the film calibration, twelve 5cm x 5cm pieces were cut from

lot #04141401. One film was left unexposed (0 cGy) and the remaining were irradiated with doses ranging from 10 cGy to 600 cGy using a 6 MV photon beam from a Varian Clinac IX/ Triology linear accelerator (Varian Medical Systems, Palo Alto, CA) . Each piece was placed centrally in a 30cm × 30cm × 11 cm stack of Solid Water® (Gammex RMI, Middleton, WI, USA) at a depth of 1. 5 cm with 100 cm source-to-axis distance (SAD) (Fig. 2.2). The field size was 10×10 cm^2.

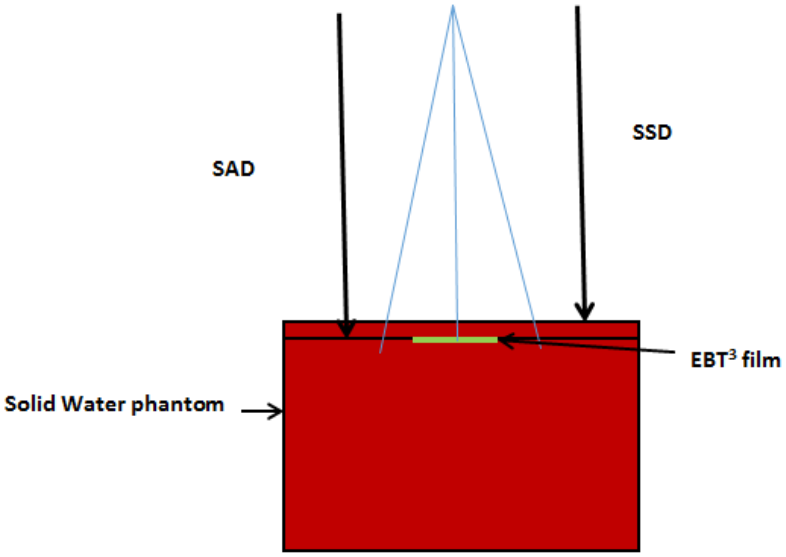

Figure 2.2: Experimental setup for film calibration and uncertainty analysis. Each 5×5 cm^2 piece of EBT3 film was placed centrally in a 30cm ×30cm × 11cm stack of Solid Water phantom at a depth of 1.5 cm with 100 cm source-to-axis distance (SAD). The field size was 10 × 10 cm^2.

The dose delivered to the films was calculated from the delivered M U. A 0.6 cc cylindrical ion chamber was placed at a depth of 5 cm in the Solid Water phantom with 100 cm SAD and was irradiated with 100 MU. Three readings were obtained and the average was calculated. The average was corrected for the effect of temperature and pressure to obtain the current machine output. The deviation of the machine output from calibration (Oc) was obtained by taking a ratio of current machine output and that at machine calibration. The delivered dose was calculated by multiplying the MU with Oc.

2.3.2 Scanning protocol and analysis

A flatbed scanner Epson 10000XL scanner (SEIKO EPSON Corporation, Nagana, Japan) and its accompanying software EPSON SCAN v3.45E was used to digitize all films. The film pieces were scanned one at a time, 24±2 hours after irradiation. The

scanner was switched on approximately 30 minutes prior to use to allow the scanner to warm up. Three empty scans were performed as part of the warm up procedure before scanning the films. The film pieces were placed at the centre of the scanner to minimize the uncertainty due to non-uniformity of the scanner. The images were acquired in transmission mode and 48-bit colour with a resolution of 75 dpi and were saved in tagged image file format (TIFF). Gloves were worn at all times when handling the film.

ImagJ 1.47v software was used for the film analysis [58]. From the TPS study it was found that the skin doses were calculated to be in the range of 150 cGy to 200 cGy. Hence a dose range of 0-600 cGy was used to create a calibration curve. To select the most sensitive colour channel for doses in this range, the images were split into three channels – red, green and blue. The mean pixel values from each channel were extracted using a region of interest (ROI) of 5 × 5 mm^2 at the centre of the film. This ensured that the possible artefacts due to the cutting of the film at the film edge were avoided. The optical density was calculated using the following equation:

$$Optical\ density\ (OD) = -log_{10}(\frac{mean\ pixel\ value}{65535}) \qquad \text{Eq. 3}$$

The net optical density (netOD) values were obtained by subtracting the OD of the background (unexposed) film. The netOD for each channel was plotted as a function of dose [58]. It was found that the red channel had a higher sensitivity for dose in the range of interest (Fig.2.3). Hence in this work, only the red channel data was used for subsequent analysis.

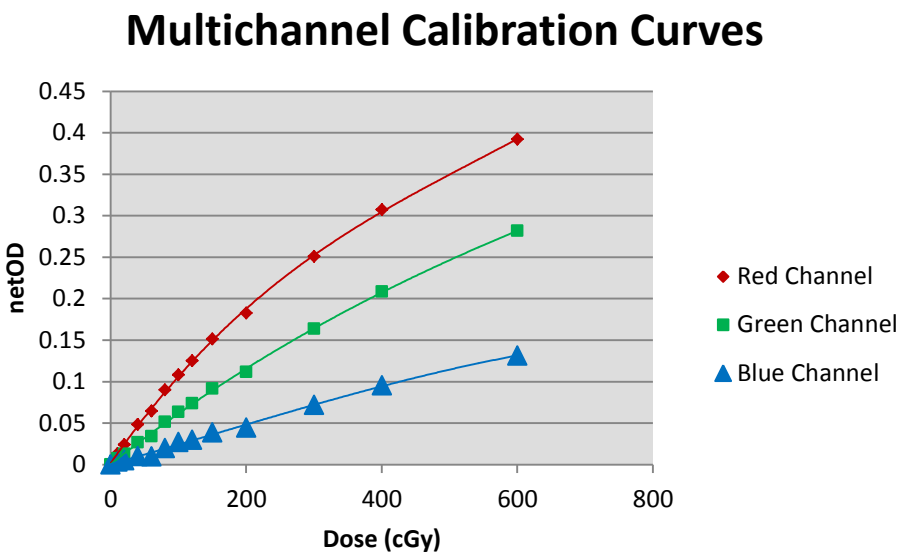

Figure 2.3: Response of red, green, and blue channels to dose below 600 cGy.

2.3.3 Uncertainty of EBT3 film

The sources of uncertainty in the film dosimetry include exposure to ambient light, post-irradiation darkening, scanner non-uniformity, orientation of film, film uniformity, scanner reproducibility, and inter-sheet variation. To reduce the effect of ambient light, the films were kept in light-tight packets. The uncertainty in scanner non-uniformity was minimized by scanning at the centre of the scanner. Several studies reported that the differences in netOD between portrait and landscape directions are significant (up to 4.5 % difference) [44, 59]. It was also shown that differences in netOD due to film face-up/ face-down orientation were less than 0.7% [44, 59, 43]. Hence to minimize these uncertainties, the film pieces were marked to ensure that they were scanned in the landscape direction with face-up. Borca et al. showed that the variation in netOD was less than 0.008 (dimensionless) if the films were scanned between 2 hours and 24 hours after irradiation [44]. Dreindl et.al demonstrated that the deviations in netOD after 20 hours were 0.9% for 30 cGy and were reduced to negligible values at higher dose levels (≥ 200 cGy) [59]. Hence to reduce the uncertainty due to post-darkening, the films were digitized after 24±2 hours.

Uncertainty in the film uniformity was quantified by measuring the optical density of ten film pieces irradiated to the same dose one after the other. A single EBT3 film

was cut into ten pieces, with dimensions 5 × 5 cm^2 and irradiated with 200 cGy in Solid Water phantom (30 × 30 × 15 cm^3) at a depth of 1.5 cm with 100 cm SAD in 10 × 10 cm^2 field size. The inter-sheet variation was analyzed by measuring the OD of three film pieces taken from three different sheets and exposed to the same dose in the aforementioned experimental setup (Fig. 2.2). The single film scanner reading reproducibility was quantified by scanning the same piece of film ten times at the centre of scanner [60].

2.3.4 Surface dose measurement with parallel plate chamber and Gafchromic film EBT3

Extrapolation chambers give the most accurate surface dose. However, as they are not available in every centre, parallel plate ionization chambers are commonly used [36, 34]. As extrapolation chambers are not available at ACH, surface dose measured with parallel plate chamber is considered as the gold standard for the purpose of this study. Film is a practical solution for measuring surface dose on a phantom. However, it carries significant uncertainties as described in section 1.3.2.3. And a strict protocol has to follow to minimize the uncertainties. Therefore parallel plate chamber measurements were made to verify the results obtained by film.

2.3.4.1 Parallel plate chamber measurement

All dose measurements were performed for a 6 MV beam with 100 cm source-to-surface distance (SSD), 10X10 cm^2 field size and at different depths using a 30 x 30 x 11 cm^3 Solid Water phantom (Gammex RMI®, Middleton, USA). A parallel plate ionization chamber (PPC40, Scanditronix Wellhöfer, Germany) with a Unidose electrometer (PTW FREIBURG, Freiburg, Germany) was used to record the dose. The plate separation and sidewall-to-collector distance (guard ring width) of the parallel plate chamber were 2 mm and 3.8 mm respectively (Fig.2.4). The effective point of measurement was defined at 1 mm below the outer surface of the chamber. To correct the polarity effect, the average reading was calculated as follows-

$$Q_{avg} = \frac{Q_+ + Q_-}{2} \qquad \text{Eq. 4}$$

where Q_+ = dose measured with positive polarity, Q_- = dose measured with negative polarity [34, 35].

The average of three readings for each depth was calculated for both polarities. Q_{avg} was normalised to 100% at the maximum dose depth.

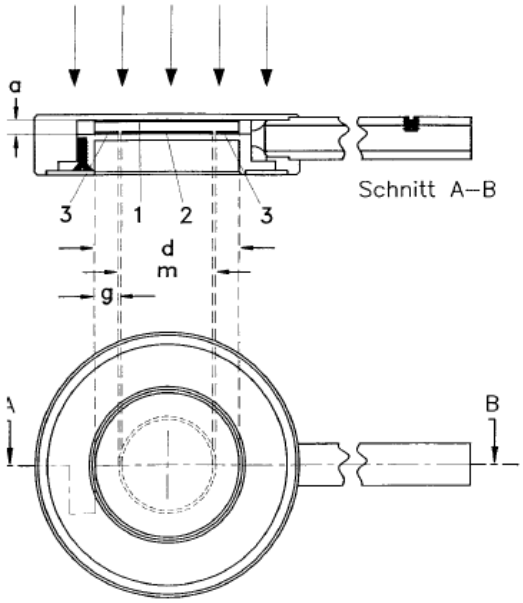

Figure 2.4: Schematic diagram of parallel plate chamber. 1: the polarizing electrode. 2: the measuring electrode. 3: the guard ring. a: the height (electrode separation) of the air cavity. D: the diameter of the polarizing electrode. M: the diameter of the collecting electrode. G: the width of the guard ring [61].

The measured percent depth dose was corrected for the chamber characteristic as follows-

$$P'(d,E) = P(d,E) - \xi(0,E)Ie^{-\alpha(d/dmax)} \qquad \text{Eq. 5}$$

$\xi(0,E)$ = energy dependent chamber factor = [-1.666 + (1.982IR)][C-15.8]

where IR = the ratio of ionization at the depth of 20 and 10 cm measured at a constant source-to-detector distance and 10X10 cm^2 field size (0.667 for the 6 MV beam)

P' (d, E) = corrected percent depth dose

P (d, E) = relative depth ionization

C= sidewall-collector distance (3.8 mm for PPC40 chamber)

L = plate separation (2 mm for PPC40 chamber)

E = energy

α= the constant of proportionality equal to the fractional change in the over response in percent, of the chamber per unit change in d/dmax = 5.5

d = depth of the effective point of measurement below the phantom surface

$\xi(0,E)Ie^{-\alpha(d/dmax)}$ = calculated correction factors

-1.666, 1.982 and 15.8 = constants from graph of percent of maximum ionization per millimetre of plate separation at the phantom surface plotted as a function of guard width or collector edge- sidewall distance [34, 35].

2.3.4.2 Film measurements

For the surface dose measurement, one piece of film (5 x 5 cm^2) was placed on the surface of the Solid Water phantom and 200 cGy was delivered using a 6 MV photon beam at 100 source-to-surface distance (SSD) in a 10×10 cm^2 field. Another film piece with the same dimensions was kept at 1.5 cm depth and was irradiated with 200 cGy of 6 MV photon beam with the same SSD and field size.

2.3.5 Evaluation of surface doses in the original plan with bolus and new no bolus plans

In this investigation the surface doses delivered in the original plan with bolus and one 'no bolus' plan from 'PTV coverage optimization' study for two patients were verified using film dosimetry. The selected 'no bolus' plans had better PTV coverage and skin ROI dose than other 'no bolus' plans in that study. Both plans were '2 arcs VMAT' plans.

2.3.5.1 Phantom

The Multiplug cavity accessory of ArcCheck phantom (Sun Nuclear Corporation) was used as a phantom as it is cylindrical in shape and simulates the head and neck geometry. Its physical density is 1.045 g/cm^3. It has a bezel made of clear acrylic with angle markers from 0° to 360°. A 0.04 cc cylindrical ionization chamber can be inserted into the Multiplug cavity to measure the point dose at a particular location [62, 63].

Using the angle markers on the bezel points were marked at 10° intervals on the surface of the phantom at a distance of 15 cm from the bezel in the superior/inferior direction as shown in Fig.2.5a. Radio-opaque ball bearings (BB) were placed on these points to help with localization and the phantom was scanned using departmental protocol for head and neck CT scanning. The phantom CT images were then imported into Pinnacle^3 and a reference point 'CT Ref' was placed on the CT zero slice. Its axes intersected the BBs at 0˚, 90˚, and 270˚. An 'Isocentre_Phantom' point was created at the same position. An external contour and BB contours were generated. The density of BBs was overridden to 0 (density of air) since they would not be present for the film measurements. The physical density of the phantom was set to 1.045 g/cm^3 [62].

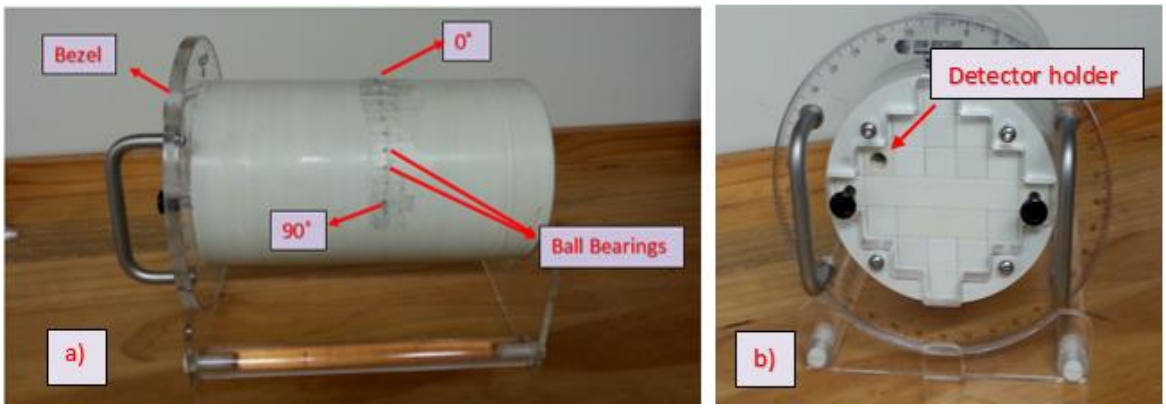

Figure 2.5: a) ArcCheck Multiplug insert. Ball bearings were placed at 10˚ intervals along a line at 15 cm distance from the bezel. The ball bearings at angles 0˚, 90˚ and 270˚ (not seen in figure) were used for phantom setup on treatment couch. b) Detector holder for 0.04 cc chamber. The position of detector can be changed.

2.3.5.2 Transferring patient plans to the phantom

QA plans were created by transferring the patient plans to the phantom CT image dataset using departmental VMAT QA protocol. The treatment beams were attached to a new point 'Shift Iso' so that the plan could more closely resemble the patient plan. The location of 'Shift Iso' was adjusted such that the bolus contour was on the external of the phantom and the skin contour was adjacent to the bolus contour as shown in Fig. 2.6. It was ensured that the bolus contour was on the external contour on all slices. Wherever required, the position of both bolus and skin contours were adjusted.

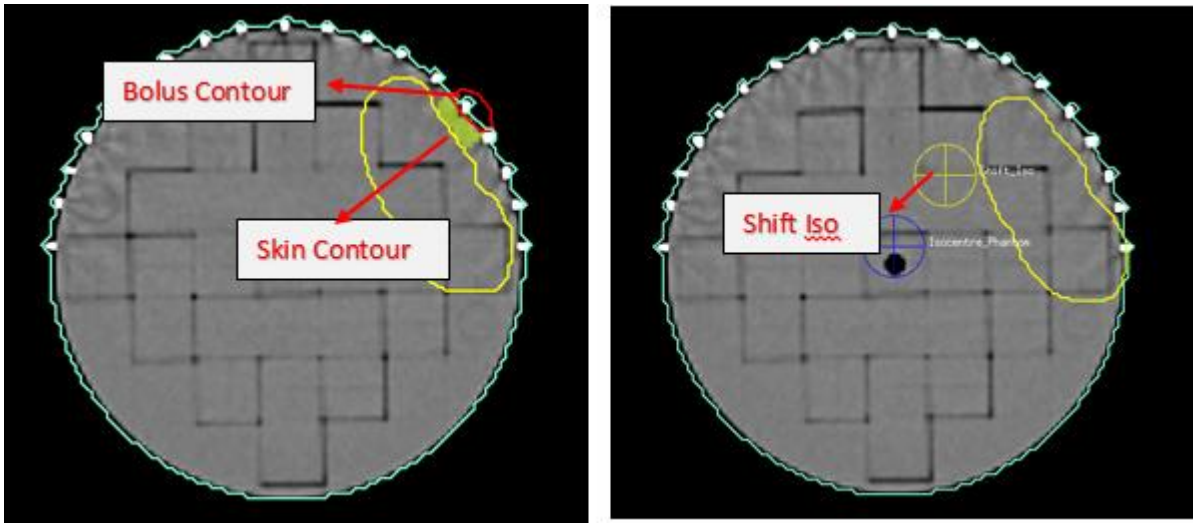

Figure 2.6 : The position of 'Shift Iso' was adjusted such that the bolus contour was on the external contour of the phantom.

The new isocentre was named as 'Shift Iso'. The distance between the centre of the phantom ('Isocentre_Phantom) and 'Shift Iso' in all three directions (anterior-posterior, lateral, and superior-inferior) was calculated from the co-ordinates of the two points. Then the couch shifts required to bring the 'Shift Iso' point at the radiation isocentre at the time of plan delivery were calculated. Table 2.3 illustrates the couch shifts required for one plan.

Table 2.3 : Calculation of couch shifts required to bring 'Shift Iso' at the linac isocentre. In this example the couch was moved towards phantom's right by 1.7 cm (lateral shift) and down by 2.3 cm (ant-post shift). There was no movement in sup-inf direction.

	Lateral (cm)	Ant-post (cm)	Sup-inf (cm)
Isocentre_Phantom	-0.79	-2.38	0
Shift Iso	0.86	-0.04	0
Couch Shifts	-1.7	-2.3	0

It was ensured that the density of 'Bolus' was 1 and 0 in the original plan with bolus and 'no-bolus' plans respectively. The dose was re-computed. A dose reference point ('Dose Ref') was to be measured at delivery for the following reasons. A point dose measurement by a cylindrical ion chamber in a high dose, low dose gradient region is often used for patient plan verification as it givens a consistent and reproducible measurement. Therefore the aim was to verify surface dose measurement with film with a point dose measurement close to the center of the PTV (Fig. 2.7). The dose at 'Dose Ref' point was noted from the 'Point of Interest Dose Table' within the TPS. A

dose line profile tool was used to obtain the surface dose on each slice containing the 'Bolus' and 'Skin' contours and an average was calculated to get the planned surface dose.

Figure 2.7: 'Dose Ref' point (red circle) was placed in a high dose, low dose gradient region to measure point dose for verification of plan delivery accuracy.

2.3.5.3 Location and dimensions of bolus and/or film

The location of the bolus and/or film on the phantom was determined from the BBs. For example, in Fig. 2.6 the 'Bolus' contour is on the fifth BB on the left side of the phantom (right side of observer). This corresponds to a 50˚ angle. Hence during treatment delivery the bolus and/or film was placed near the 50˚ mark. The distance between the start of bolus and the zero slice (the slice containing the 'Isocentre_Phantom' point) was measured to determine the position of bolus in sup-inf direction.

The number of slices containing bolus were counted and was multiplied by 0.2 cm (thickness of one slice) to obtain its length in superior-inferior direction. The width of the bolus in anterior-posterior direction was measured. Thus the dimensions of bolus used for each patient were determined and film pieces of appropriate size were cut for film dosimetry. To cover the film completely, boluses of bigger dimensions (length of film + 0.4 cm in superior-inferior direction, and width of film + 0.5 cm in anterior-posterior direction) were prepared.

2.3.5.4 Treatment delivery

The phantom was set up on the treatment couch by aligning the 90° and 270° marks with the wall lasers and the 0° mark with the roof laser to match the position at CT.

The appropriate couch shifts were applied to bring the 'Shift_Iso' point at the isocentre. A 0.04 cc cylindrical ionization chamber was inserted in the detector holder to measure the dose at 'Dose Ref' point. Radiochromic EBT3 film was placed on the region of interest and was secured using tape. It was ensured that the tape covered the film no more than 0.5 cm from the edges. Bolus was placed on the film during the delivery of original plans with bolus (Fig. 2.8b).

Each plan was delivered twice and the doses were recorded with film and the ion chamber. The ion chamber measurements were corrected for various parameters and converted into the absorbed dose by applying a calibration factor. Surface doses were obtained from film measurements using the calibration curve.

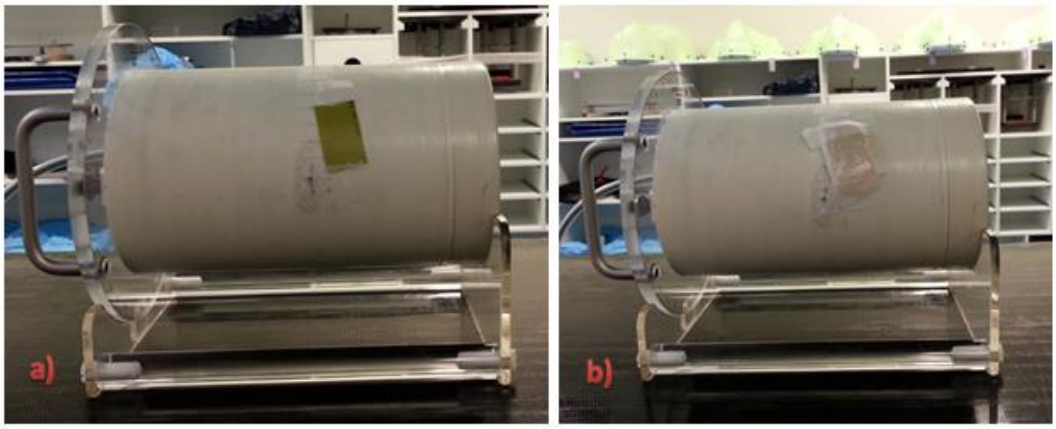

Figure 2.8: a) Phantom set up on the treatment couch with EBT3 film placed at area of interest. b) Bolus completely covered the film during the delivery of original plan with bolus.

3. Results and Discussion

This chapter is divided into two sections - treatment planning study and film dosimetry. The treatment planning section includes the analysis of the treatment plans in terms of the planning target volume (PTV) coverage and skin dose. The dosimetry section includes results of the film calibration as well as an analysis of the uncertainties in film dosimetry. Surface dose measured with film was validated by the surface dose measured with a parallel plate chamber. Analysis of the surface dose measurements using a parallel plate chamber and film is given, and finally the surface dose measured by film on the phantom for patient plans are evaluated.

3.1 Treatment Planning Study

As stated in section 2.2.2, the treatment planning study was divided into two parts – optimising the PTV coverage and optimising the skin ROI dose.

3.1.1 Optimising the PTV coverage

In all patient plans, the PTV was extended up to the patient's surface to treat the scar tissue (Fig. 3.1 a). The required build-up was provided by bolus. Hence, the optimizer could easily deliver dose near the surface without causing hotspots in other parts of the plan. However, as the bolus was removed in the new no bolus plans, a part of the PTV was shifted into the build-up region. Therefore, as mentioned in section 2.2.1, a 3 mm strip of tissue closest to the patient's surface was removed from the PTV to prevent Pinnacle^3 from driving the optimiser too hard in the build-up region, which can lead to over-modulated plans and poor quality dose distribution (Fig. 3.1 b). Hence, the PTVs in the original plan with bolus and the new no bolus plans were slightly different. However, as the goal of the treatment was to treat the PTV extended up to the patient's surface, doses to this PTV were reported for all patients.

ICRU states that the PTV should be covered with at least with 95% of prescribed dose in order to deliver adequate dose to the CTV [56]. Hence, in this study, plans without bolus were produced to achieve at least 95% isodose coverage of the PTV. Subsequently the effect on dose to the skin ROI was assessed.

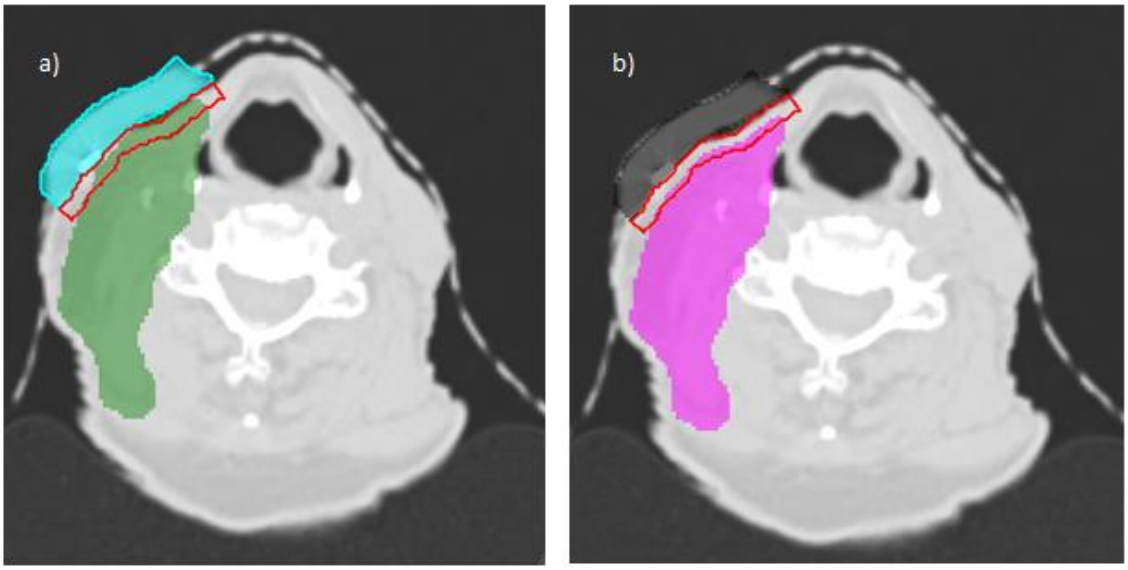

Figure 3.1 : a) The PTV (green colourwash) in the original plan with bolus was extended up to the patient's surface. Doses to this PTV were reported for all patients. b) A 3 mm strip of tissue closest to the patient's surface was removed from the PTV to avoid optimization problems in the build-up region. The modified PTV is shown in purple colourwash.

The PTV coverage was quantified using a parameter known as $V_{95\%}$, which is the proportion of the target volume receiving 95% of the prescription dose. For example, "$V_{95\%}$ = 98%" means 98% of the PTV volume is receiving 95% of the prescribed dose. Based on the ICRU guidelines and discussion with the clinicians, a plan with $V_{95\%} \geq$ 95% for the PTV is clinically accepted at Auckland City Hospital (ACH). To analyse the impact of missing bolus on the skin ROI dose, the mean dose to the skin contour in each plan was normalised to the prescribed dose using Eq. 2.

3.1.1.1 Case-by-case comparison of the PTV coverage and dose to the skin

The main objectives of a treatment plan is – to achieve optimal PTV coverage ($V_{95\%} \geq$ 95%), to keep doses to the OARs within their tolerance limit, and to limit the maximum dose in the overall plan to less than 110% of the prescription dose. However, each patient is a unique case in terms of the extent of the tumour, the size and shape of the tumour and the adjacent anatomy. Hence, each patient plan is different and it can be difficult to make comparisons of planning parameters from one patient to another. In this section, the PTV coverage and dose to the skin are

evaluated on a case-by-case basis. For each patient, the no bolus plan, regardless of the technique, which best achieved the planning objectives was compared with the original bolus plan.

3.1.1.1.a Patient 1

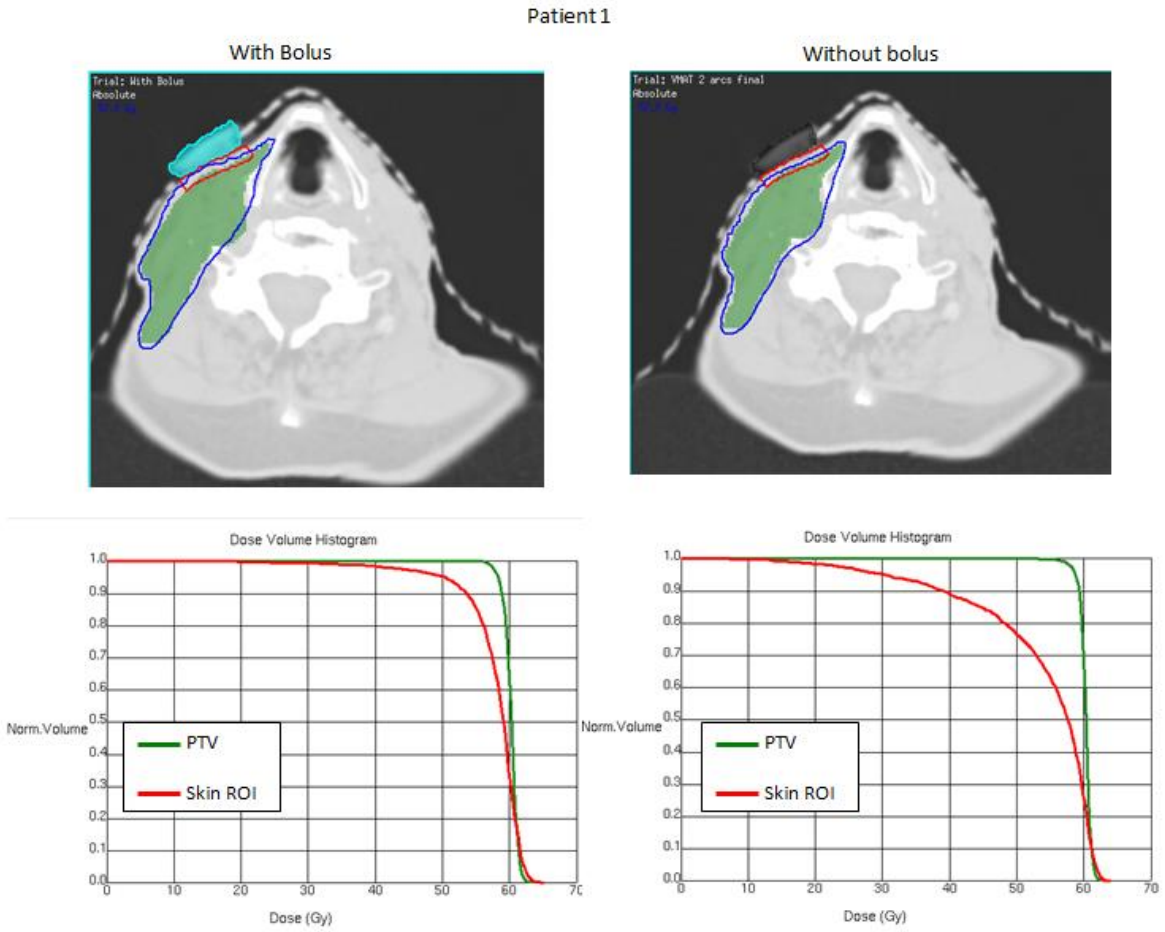

Figure 3.2 : Comparison between PTV coverage in the original IMRT plan with bolus and the new 2 full arcs VMAT plan without bolus for Patient 1. The upper panels show the PTV (green colourwash), the skin ROI (red contour) and bolus (sky blue). The 95% isodose line is shown in blue. The lower panels show the dose volume histograms (DVHs) for both plans.

The PTV coverage in the original plan with bolus and new plan without bolus was 98.9% and 97.6 % respectively. Corresponding normalized mean skin ROI doses were 96.33% and 88.67 %. As seen in Fig. 3.2, the PTV is a narrow strip and the bolus covers only a small portion of the PTV. Hence removing the bolus did not have a significant effect on the overall PTV coverage and it was possible to achieve clinically acceptable PTV coverage fairly easily.

However, it did have a major effect on the skin ROI dose. In the original plan with bolus, a large portion of the skin ROI was included in the PTV and the required build-up was provided by bolus. Hence, as seen in dose volume histogram (DVH) of the original plan with bolus, 95% of the skin ROI received at least 50 Gy. In other words, $D_{95\%}$ of the skin ROI was 50 Gy. On the other hand, $D_{95\%}$ of the skin ROI was only 30 Gy in the no bolus plan. Thus the reduction in $D_{95\%}$ was 40%. This was due to the fact that in the no bolus plan, a substantial part of the skin ROI had to be excluded from the PTV (Fig.3.1 b) to prevent Pinnacle[3] from driving the optimiser too hard in the build-up region, which can lead poor quality dose distributions. Hence, the dose to the skin dropped significantly when bolus was removed. In the simplest terms, the removal of bolus shifts part of the PTV into the build-up region, thus reducing dose to the skin ROI in that area.

3.1.1.1.b Patient 2

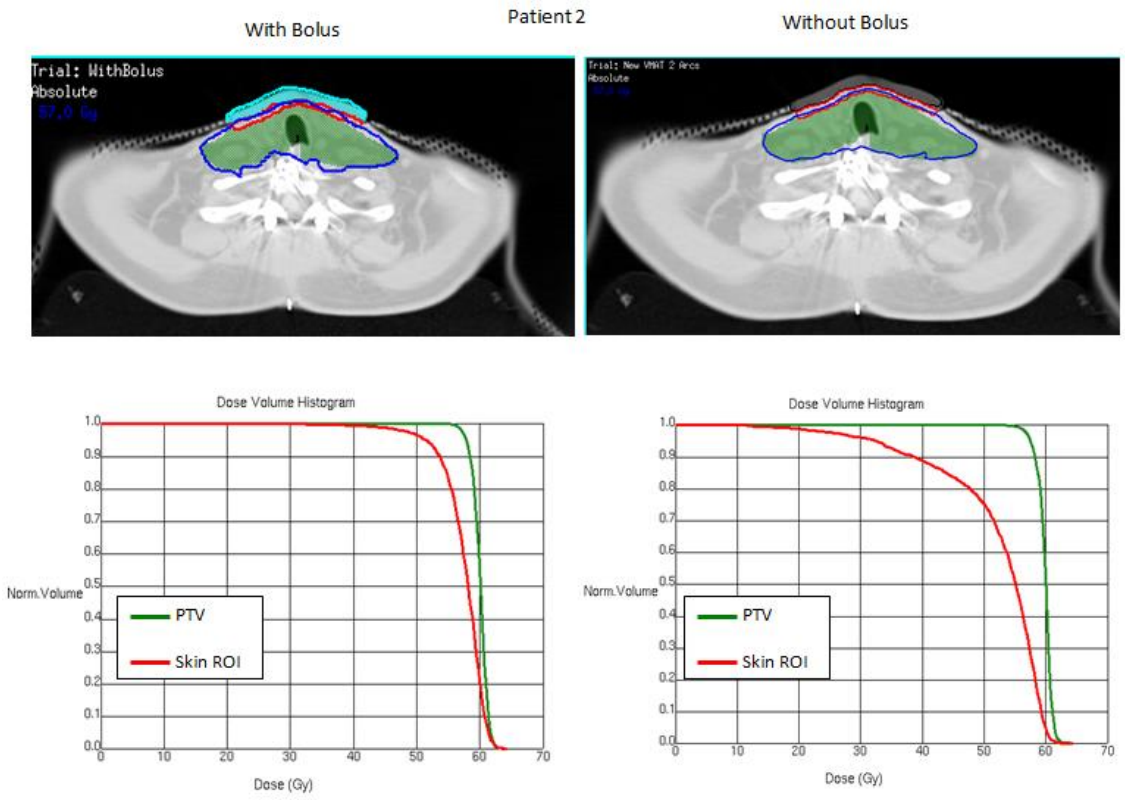

Figure 3.3: Comparison between PTV coverage in the original IMRT plan with bolus and the new 2 full arcs VMAT plan without bolus for Patient 2. The upper panels show the PTV (green colourwash), the skin ROI (red contour) and bolus (sky blue). The 95% isodose line is shown in blue. The lower panels show the dose volume histograms (DVHs) for both plans.

The PTV coverage in the original plan with bolus and new plan without bolus was 98.1% and 97.10% respectively. The corresponding normalized skin ROI doses were 95.67% and 86.50 %. In this case, the PTV was crescent shaped and extended bilaterally. The bolus was positioned centrally on the neck (Fig.3.3). The bolus did not cover the full extent of the PTV, and this may be part of the reason why there was a very small detrimental effect on the PTV coverage.

The DVH of the original bolus plan (Fig.3.3) shows that the skin $D_{95\%}$ was 52 Gy, compared with 35 Gy in the new plan without bolus, i.e. a decrease of 32.7%. Just as in patient 1, exclusion of the skin ROI from the PTV and the proximity of the PTV to the surface in the absence of bolus resulted in lower dose to the skin.

3.1.1.1.c Patient 3

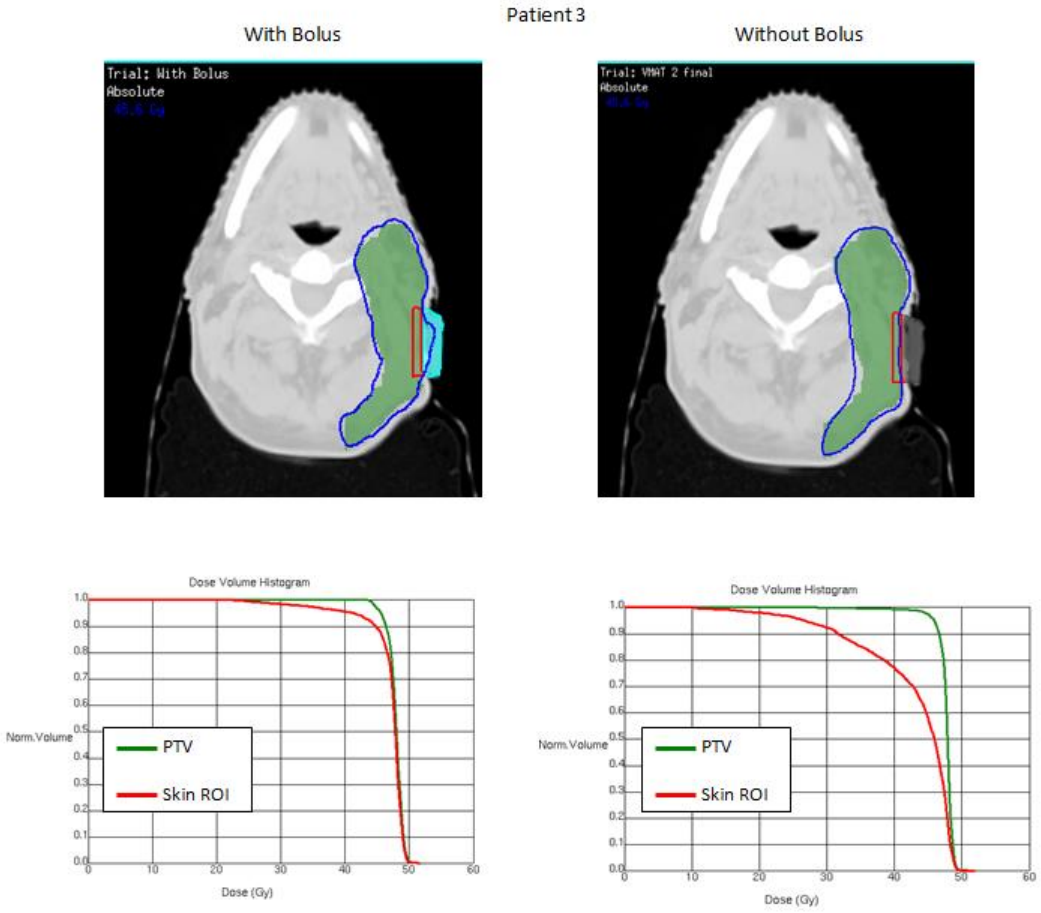

Figure 3.4: Comparison between PTV coverage in the original IMRT plan with bolus and the new 2 full arcs VMAT plan without bolus for Patient 3. The upper panels show the PTV (green colourwash), the skin ROI (red contour) and bolus (sky blue). The 95% isodose line is shown in blue. The lower panels show the dose volume histograms (DVHs) for both plans.

The PTV coverage in the new plan without bolus was marginally better than the PTV coverage in the original plan with bolus (95.80% and 94.80% respectively). In this case, an OAR (left brachial plexus) was overlapping the PTV (Fig. 3.5). Brachial plexus is the network of nerves that controls the movement and sensation in the upper limbs. In the original bolus plan, the PTV coverage had been compromised to limit the dose to the left brachial plexus. Based on the Quantitative Analysis of Normal Tissue Effects in the Clinic (QUANTEC) guidelines, for the prescribed dose of 48 Gy to the PTV, the tolerance limit for brachial plexus was 48 Gy. In the new no bolus plan, both objectives ($V_{95\%}$ for PTV > 95% and dose to brachial plexus (47.5 Gy) within tolerance limit) were achieved. This is most likely to be a result of the treatment technique (2 full arcs VMAT) used in the new no bolus plan. A VMAT plan with multiple arcs has more control points than single arc VMAT as well as IMRT which means that there is a much higher number of possible MLC positions and therefore a higher degree of modulation resulting in better plan quality, especially for a complex-shaped target volume [64, 65].

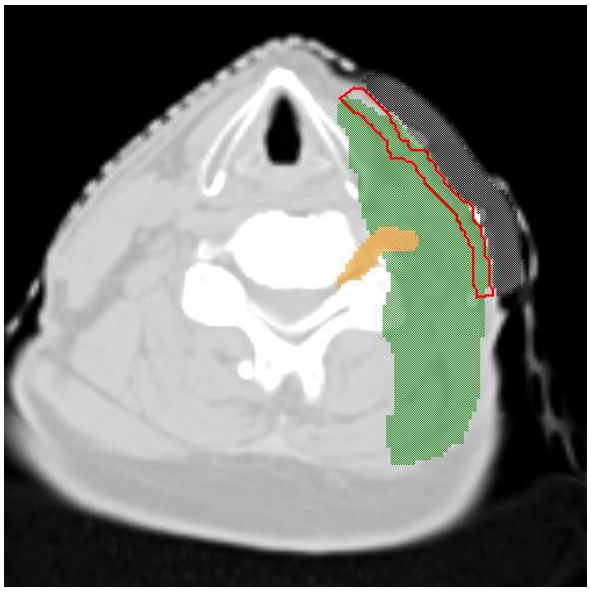

Figure 3.5: Left brachial plexus (orange colourwash) overlapped the PTV (green colourwash).

However, as with the previous cases the skins ROI dose in the new no bolus plan was considerably lower than that in the original plan with bolus (88.75% and 97.50% respectively). Skin $D_{95\%}$ in the original plan was 42 Gy compared with a very significantly reduced 27 Gy in the new plan. A considerable part of the skin ROI was

included in the PTV in the original plan. Hence 95% of its volume received high dose. However, as stated in earlier cases, removal of a major portion of the skin ROI from the PTV and the closeness of the PTV to the surface in the absence of bolus caused lower doses to the skin.

3.1.1.1.d Patient 4

The PTV coverage in the original plan with bolus and new plan without bolus was 98.1% and 99.40% respectively. Corresponding normalized skin ROI doses were 96.44% and 89.33%. The PTV was on a narrow strip on the left side of the patient and was long (16.6 cm) in superior-inferior direction. In comparison to this, the length of the bolus was 3 cm and as seen in Fig. 3.6, it covered only a very small part of the PTV in anterior –posterior direction. The volume of PTV was 340.88 cm^3 whilst volume of the skin ROI was 3.37 cm^3 i.e. the skin ROI was very small compared to the PTV. This may clarify the reason why removing the bolus did not have any effect on the overall PTV coverage and it was possible to achieve clinically acceptable PTV coverage fairly easily. However, as observed in previous case studies, it did have a major effect on the skin ROI dose. $D_{95\%}$ of the skin ROI in the original plan with bolus and the new no bolus plan was 38 Gy and 25 Gy respectively. The decrease in $D_{95\%}$ (21.9 %) can be attributed to the exclusion of the skin ROI from the PTV and the proximity of the PTV to the surface in the absence of bolus.

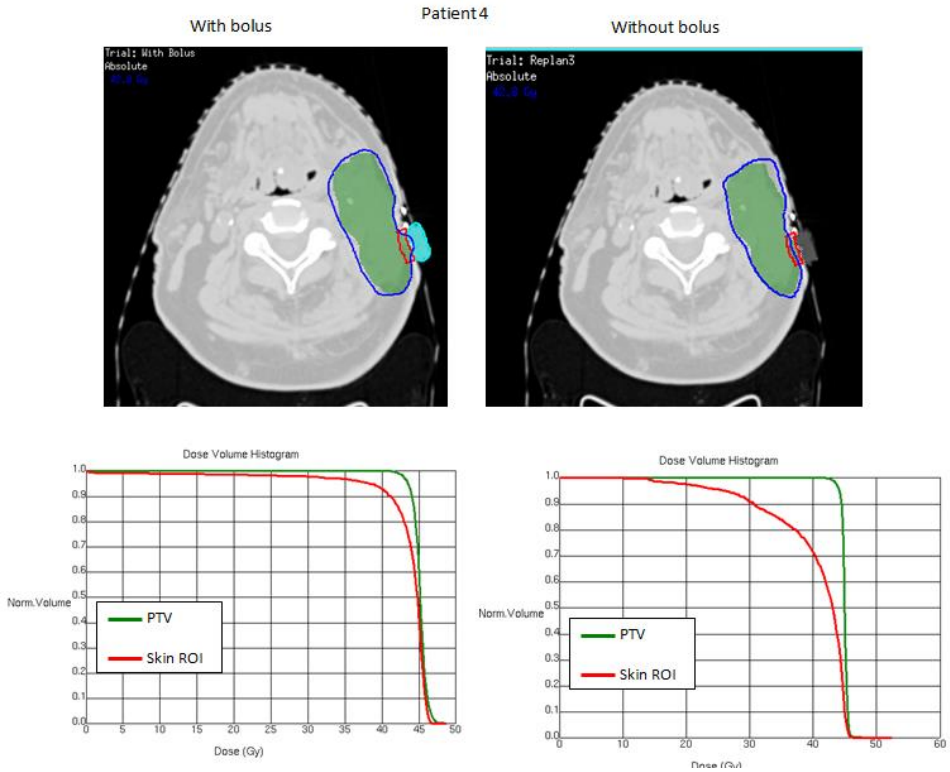

Figure 3.6: Comparison between PTV coverage in the original IMRT plan with bolus and the new IMRT plan without bolus for Patient 4. The upper panels show the PTV (green colourwash), the skin ROI (red contour) and bolus (sky blue). The 95% isodose line is shown in blue. The lower panels show the dose volume histograms (DVHs) for both plans.

3.1.1.1.e Patient 5

The PTV coverage in the original plan with bolus and the new no bolus plan was 98.2% and 97.70% respectively. Corresponding normalized skin ROI doses were 99.83% and 94.00% respectively. The PTV was a long narrow strip on the left side of the patient and was much larger in length (19.6 cm) and volume (295.41 cm^3) than the bolus (length = 7.2 cm and volume = 12.31 cm^3). Hence, removing bolus may not have a significant effect on the PTV coverage.

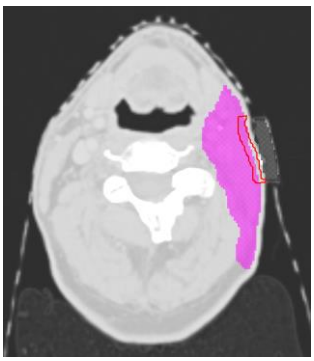

Figure 3.7 : A significant part of the skin ROI (red contour) was part of the PTV (purple colourwash) in the new non bolus plan of Patient 5.

The reduction in the skin ROI dose was less compared to previous case studies as a considerable part of the skin ROI was still included in the PTV used for optimization in the new no bolus plan (Fig. 3.7). $D_{95\%}$ of the skin ROI was 55 Gy and 45 Gy in the original plan with bolus and the new no bolus plan respectively.

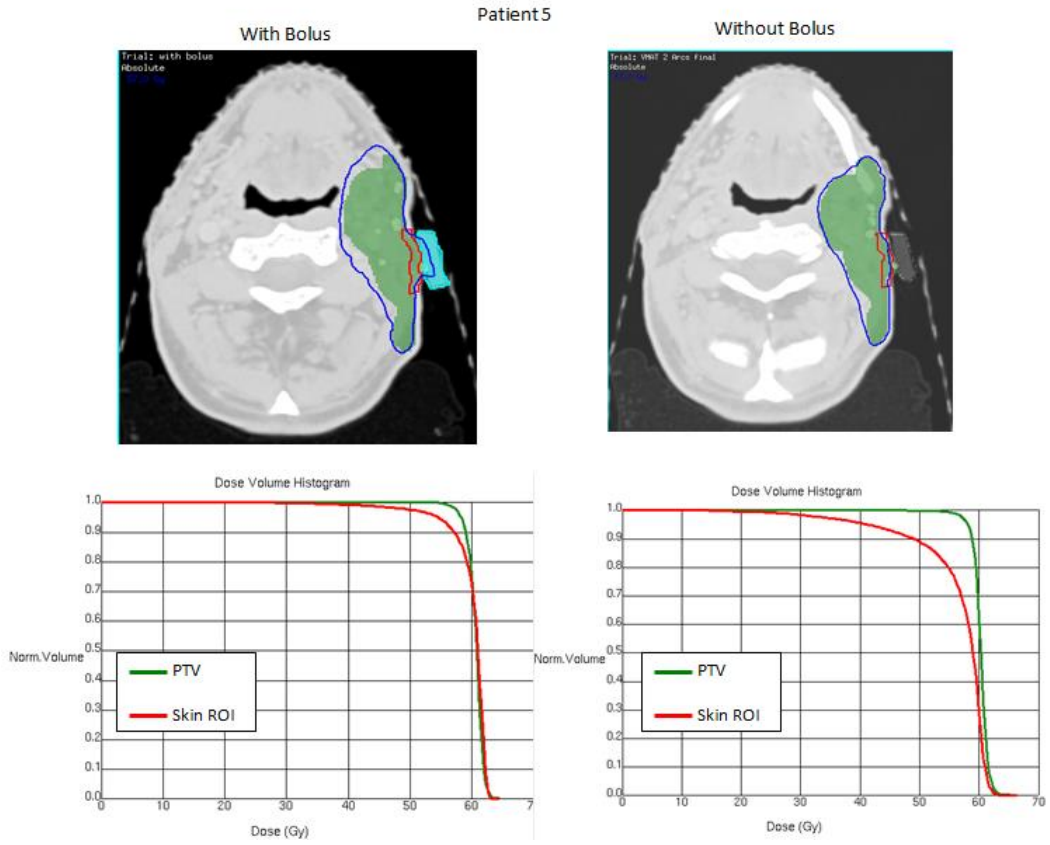

Figure 3.8: Comparison between PTV coverage in the original IMRT plan with bolus and the new 2 full arcs VMAT plan without bolus for Patient 5. The upper panels show the PTV (green colourwash), the skin ROI (red contour) and bolus (sky blue). The 95% isodose line is shown in blue. The lower panels show the dose volume histograms (DVHs) for both plans.

3.1.1.1.f Patient 6

The PTV coverage in the original plan with bolus and new plan without bolus was 99.0% and 97.10% respectively. Corresponding skin ROI doses were 100% and 88.50%. The PTV extended bilaterally and the bolus covered only a small portion on the neck. Hence it was still possible to achieve clinically acceptable PTV coverage in absence of bolus. As observed in previous case studies, $D_{95\%}$ of the skin ROI in this case, also was considerably lower in the plan without bolus (32 Gy) as compared to the original plan with bolus (57 Gy). As the skin ROI was completely inside the PTV in the original plan with bolus, it received full dose. Conversely, it received a much

lower dose in the plan without bolus as most of it had to be excluded from the PTV as explained in previous cases.

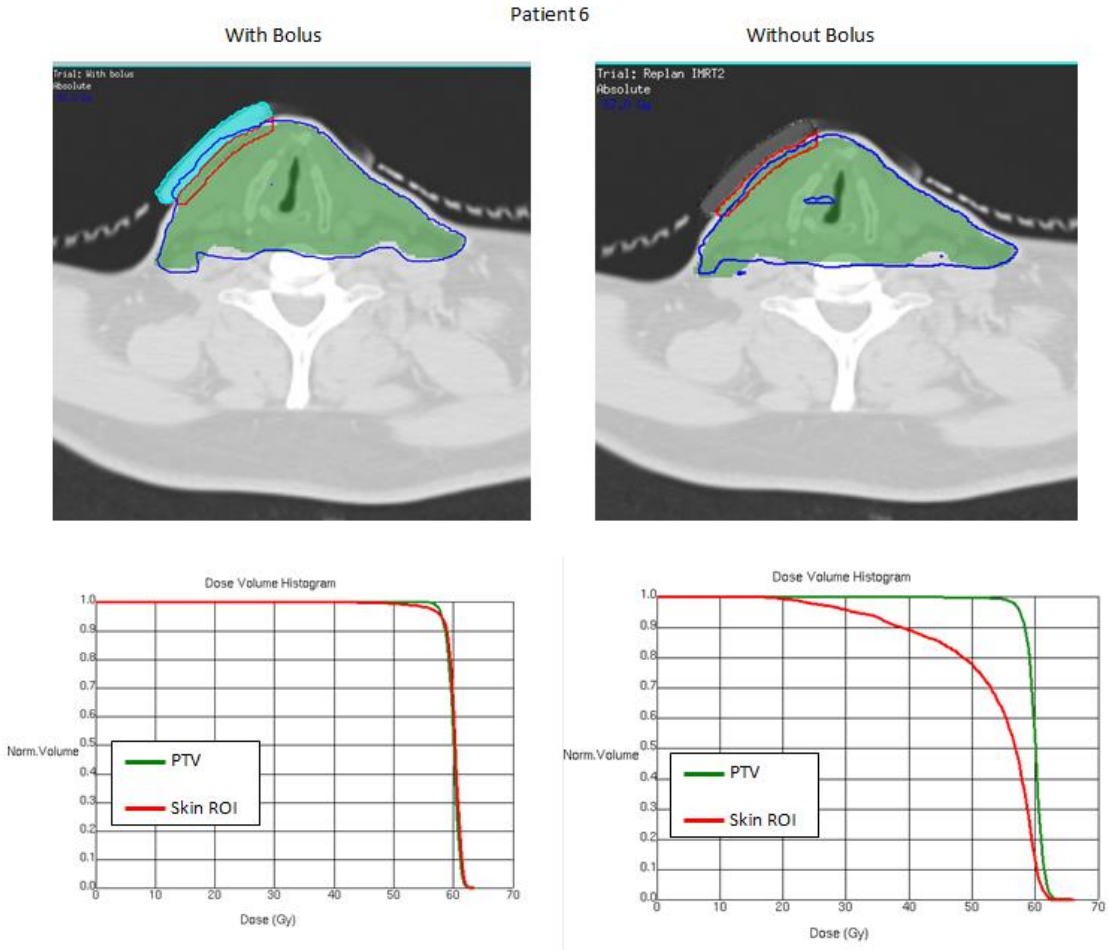

Figure 3.9: Comparison between PTV coverage in the original IMRT plan with bolus and the new 2 full arcs VMAT plan without bolus for Patient 6. The upper panels show the PTV (green colourwash), the skin ROI (red contour) and bolus (sky blue). The 95% isodose line is shown in blue. The lower panels show the dose volume histograms (DVHs) for both plans.

3.1.1.1.g Patient 7

The PTV coverage ($V_{95\%}$ = 96.90%) in the new no bolus plan was clinically acceptable. The PTV was a narrow strip on the right side of the patient's neck. The length of the bolus in the superior – inferior direction (114 mm) was comparable with the length of the PTV in superior-inferior direction (126 mm). In other words, the bolus was present almost in every slice in the CT image data. Although the bolus extended the full length of the PTV, Fig. 3.10 shows that it was small compared to the size of the PTV in the anterior-posterior direction. This may help explain why it was possible to achieve clinically acceptable PTV coverage even in absence of the bolus.

With regards to the skin, the trend noted above i.e. significant dose reduction to the skin ROI was also observed here. There was a 40% decrease in $D_{95\%}$ in the new no bolus plan (30 Gy) compared to $D_{95\%}$ in the original plan with bolus (50 Gy).

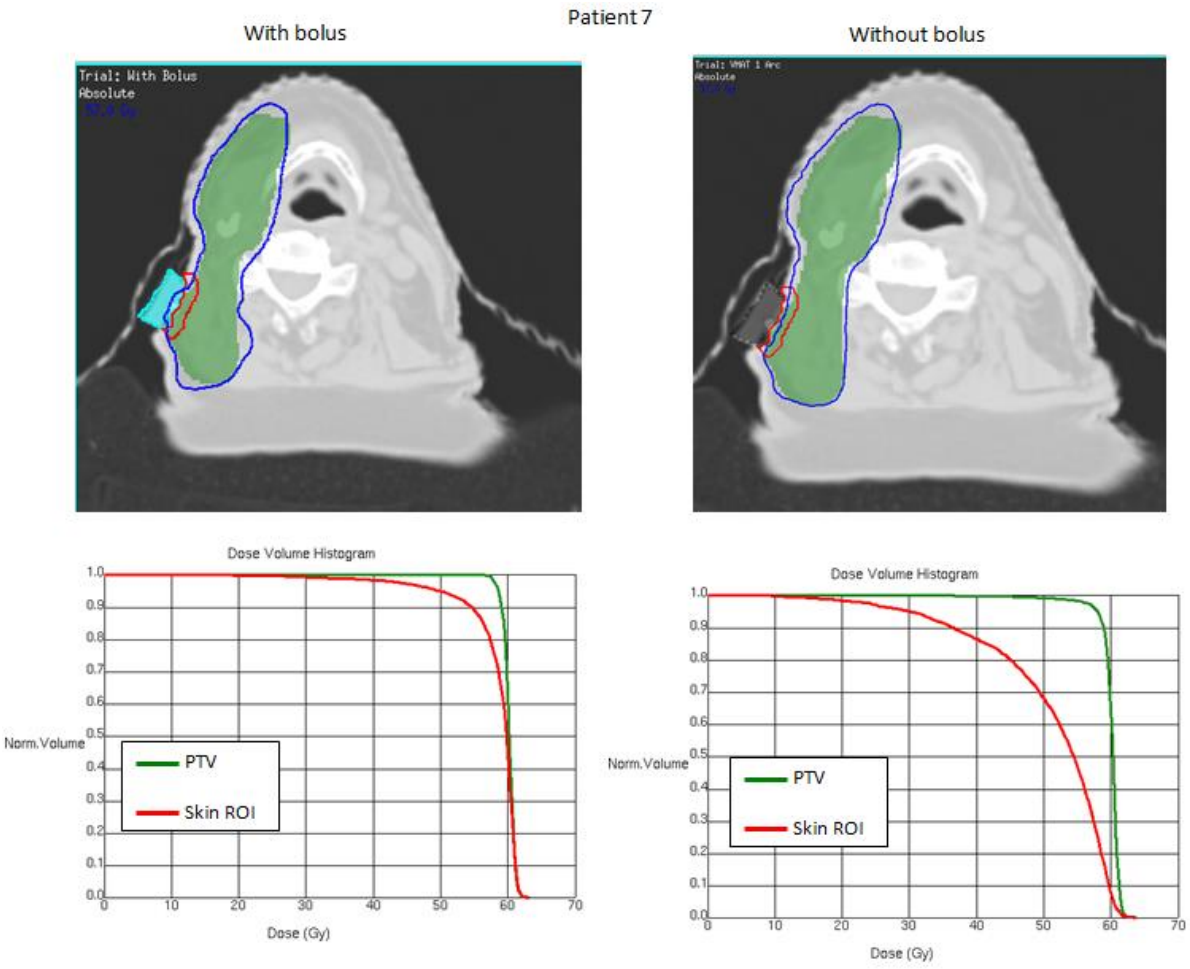

Figure 3.10: Comparison between PTV coverage in the original IMRT plan with bolus and the new 1 full arcs VMAT plan without bolus for Patient 7. The upper panels show the PTV (green colourwash), the skin ROI (red contour) and bolus (sky blue). The 95% isodose line is shown in blue. The lower panels show the dose volume histograms (DVHs) for both plans.

3.1.1.1.h Patient 8

The PTV coverage in the original plan with bolus and new plan without bolus was 99.4% and 97.50% respectively. The length of the bolus in the superior – inferior direction was 16 cm whilst the length of the PTV in superior-inferior direction was 22.6 cm. However, volume of bolus (21.5 cm^3) was small compared to volume of the PTV (392.47 cm^3). This means that although the bolus almost extended across the full length of the PTV, it was small compared to the PTV. This may help explain why

it was possible to achieve clinically acceptable PTV coverage even in the absence of the bolus.

However, the skin ROI dose was greatly reduced in the new no bolus plan. The whole skin ROI was in the PTV. Hence, it received full dose in the original plan with bolus ($D_{95\%}$ = 42 Gy). On the other hand, $D_{95\%}$ in the new plan without bolus was 25 Gy. Thus there was a 40.5% decrease in $D_{95\%}$ in the new no bolus plan.

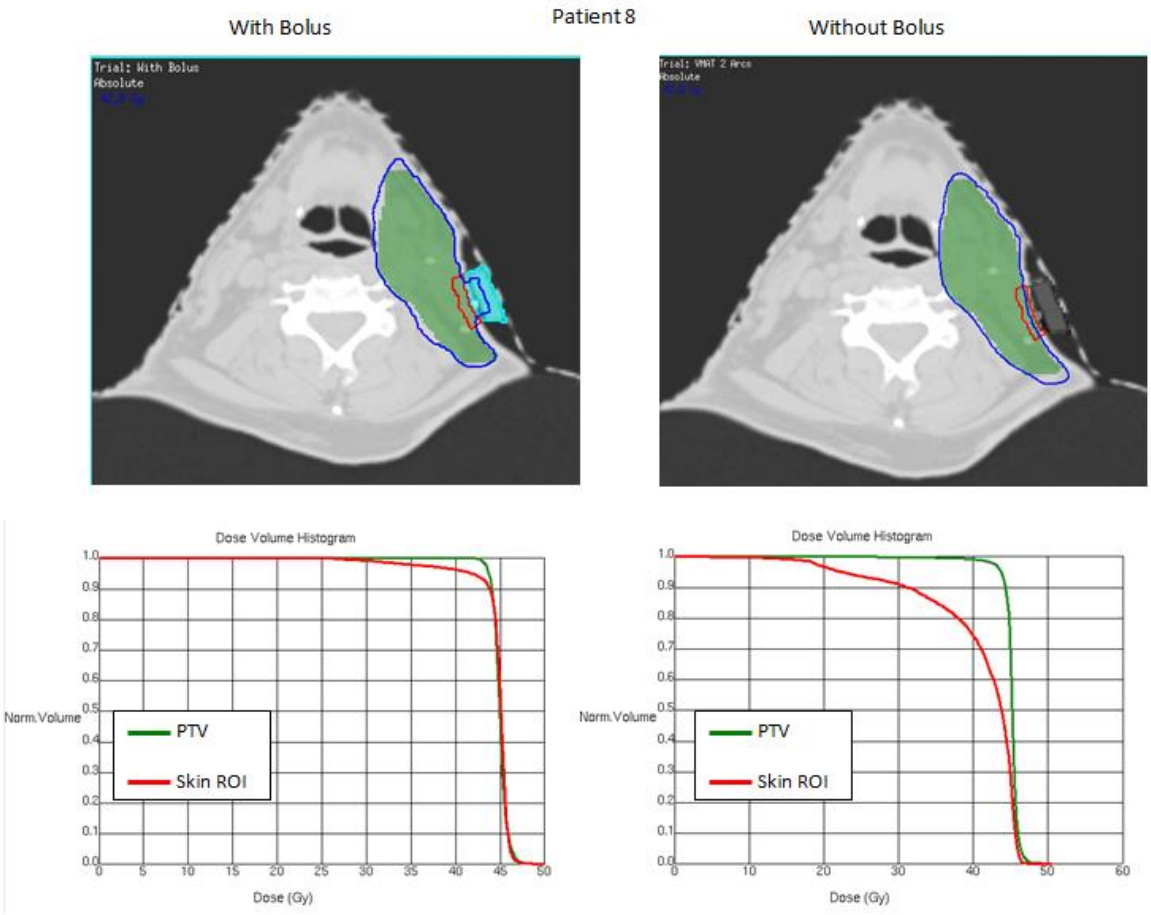

Figure 3.11: Comparison between PTV coverage in the original IMRT plan with bolus and the new 2 full arcs VMAT plan without bolus for Patient 8. The upper panels show the PTV (green colourwash), the skin ROI (red contour) and bolus (sky blue). The 95% isodose line is shown in blue. The lower panels show the dose volume histograms (DVHs) for both plans.

3.1.1.1.i Patient 9

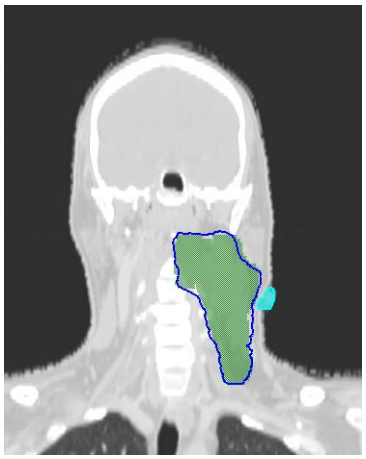

Figure 3.12: The PTV (green ROI) is extended deeper into head and neck. The bolus (blue ROI) covers only a small portion of the PTV.

The PTV coverage in the original plan with bolus and new plan without bolus was 97.6 % and 97.5% respectively. The PTV was on left side of the patient and as seen in Fig. 3.12, it was deeper in the lateral direction. Its length was 8.8 cm in superior-inferior direction and volume was 255.91 cm^3. Conversely, the length and volume of the bolus was 1.8 cm and 4.35 cm^3 respectively. Thus only a part of the PTV was covered with the bolus. This may explain why the PTV coverage was not affected in the new no bolus plan.

However, the skin ROI dose was significantly lower in the new plan without bolus. The normalised skin ROI doses were 95.43% and 83.14% in the original plan with bolus and the new no bolus plan respectively. In comparison to plans without bolus in the other case studies, dose to the skin ROI here is the lowest. As stated in section 2.2.1, usually a 3 mm strip of tissue closest to the patient surface is removed to avoid optimization problems in the build-up region. However, in this case, based on clinical consideration, the physician instructed the planners to remove a 5 mm strip of tissue. This did not cause any problem in the original plan with bolus as the skin ROI was still in the PTV (Fig.3.14 a). But, in the new no bolus plan, since the skin ROI was of 5 mm thickness, it was completely removed from the PTV (Fig.3.14 b). Therefore it was no longer possible to optimise the plan to give a high enough dose to the skin ROI.

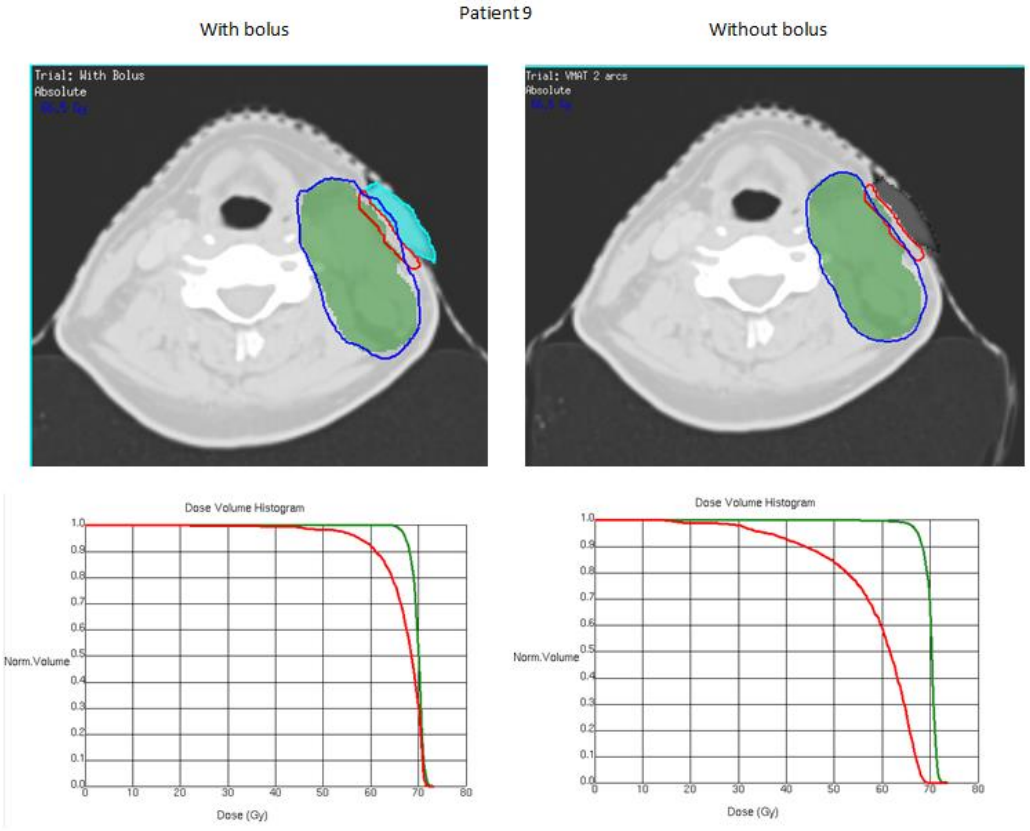

Figure 3.13: Comparison between PTV coverage in the original IMRT plan with bolus and the new 2 full arcs VMAT plan without bolus for Patient 9. The upper panels show the PTV (green colourwash), the skin ROI (red contour) and bolus (sky blue). The 95% isodose line is shown in blue. The lower panels show the dose volume histograms (DVHs) for both plans.

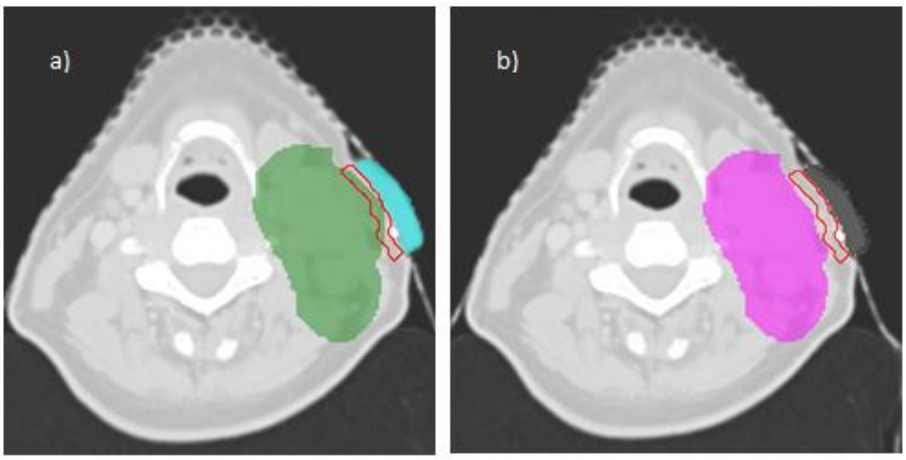

Figure 3.14: a) The skin ROI (red contour) was part of the PTV in the original IMRT plan with bolus. b) The skin ROI (red contour) was completely removed from the PTV (purple colourwash) in the new no bolus plan.

3.1.1.1.j Patient 10

The PTV coverage in the original plan with bolus and new plan without bolus was 99.2% and 98.20% respectively. The corresponding skin ROI doses were 100% and

93.67 %. The PTV was a narrow strip with length 11.6 cm in superior-inferior direction whilst the length of bolus was 4.2 cm in superior-inferior direction. As seen in Fig. 3.15, only a small part of the PTV was covered with bolus in anterior-posterior direction. Hence, removal of the bolus may not have a significant effect on the overall PTV coverage.

As seen in Fig. 3.15, the skin ROI was completely embedded inside the PTV. Hence, it was delivered full dose in the original plan with bolus ($D_{95\%}$ = 59 Gy). On the other hand, as it was excluded from the PTV in no bolus plan, $D_{95\%}$ was 35 Gy in the new no bolus plan.

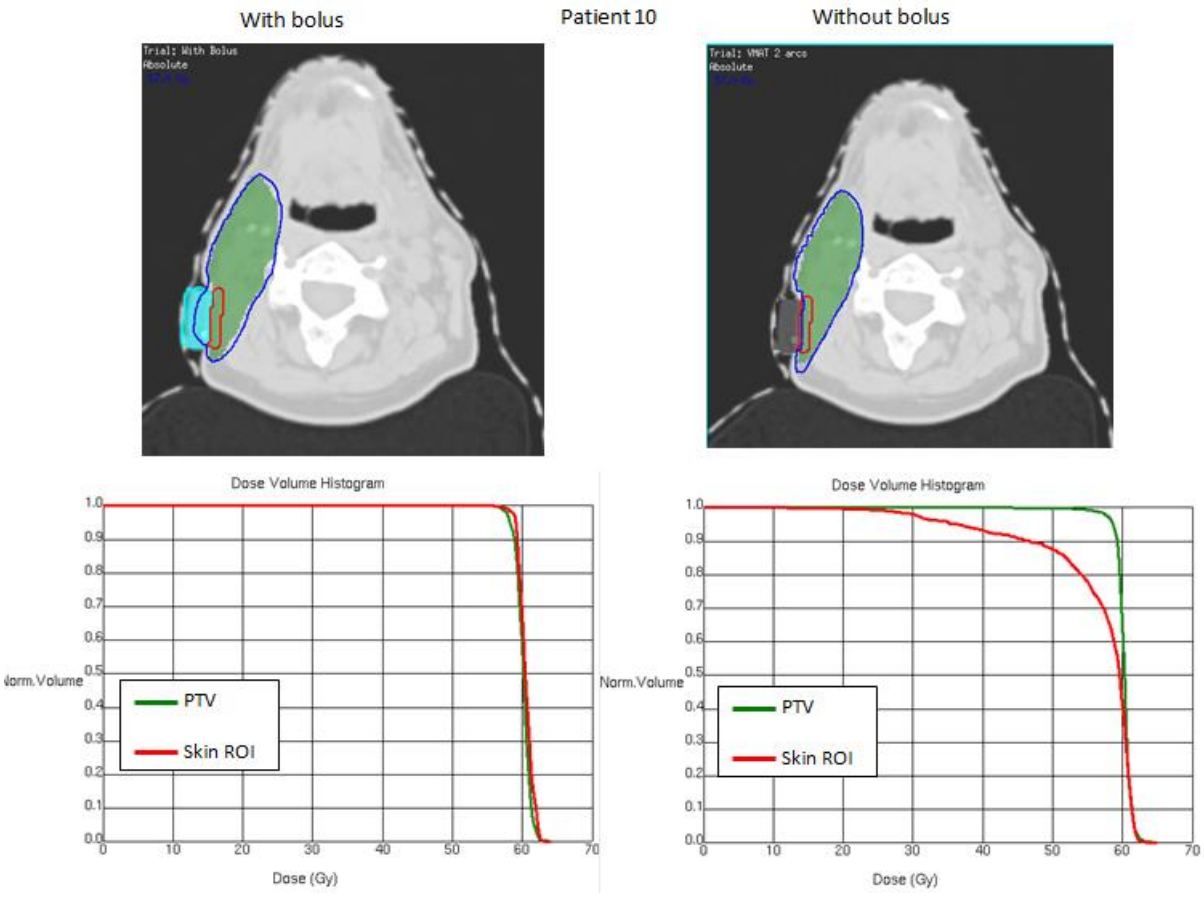

Figure 3.15: Comparison between PTV coverage in the original IMRT plan with bolus and the new 2 full arcs VMAT plan without bolus for Patient 10. The upper panels show the PTV (green colourwash), the skin ROI (red contour) and bolus (sky blue). The 95% isodose line is shown in blue. The lower panels show the dose volume histograms (DVHs) for both plans.

A common trend was observed in all case studies. The bolus was small compared to the PTV in all cases. Hence, an absence of bolus may not have affected the overall PTV coverage significantly. However, the exclusion of the skin ROI from the PTV and

proximity of the PTV to the surface in the absence of bolus may have degraded dose to the skin ROI in the new no bolus plans.

3.1.1.2 Overall comparison of the PTV coverage and dose to the skin ROI

Fig. 3.16 shows the PTV coverage obtained for the full range of advanced planning/treatment techniques used in this study for an example patient.

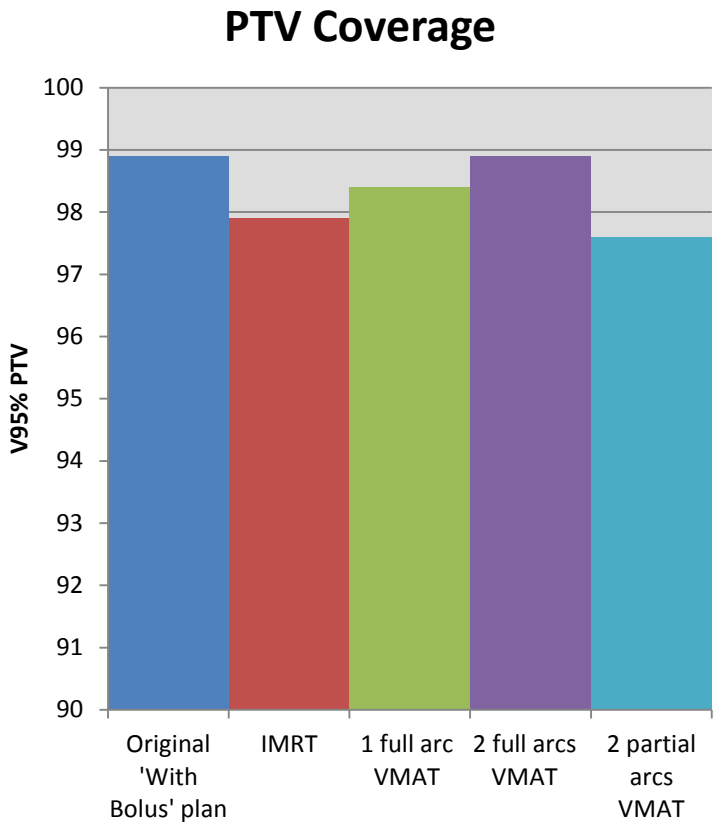

Figure 3.16: Summary of PTV coverage achieved for one patient expressed with V95%. IMRT, '1 full arc VMAT', '2 full arcs VMT' and '2 partial arcs VMAT' are all no bolus plans.

It was possible to achieve clinically acceptable coverage for all plans for this patient. In fact it was possible to cover 97% of the PTV with the 95% isodose in all cases. The PTV coverage obtained in the '2 full arcs VMAT' plan was better than the rest of the plans including the original plan with bolus.

Fig. 3.17 shows the comparison between the PTV coverage ($V_{95\%}$) in various treatment plans for all patients. For all patients, apart from one patient (Patient 3),

clinically acceptable PTV coverage ($V95_{\%} \geq 95\%$) in all no bolus plans for all patients was achieved.

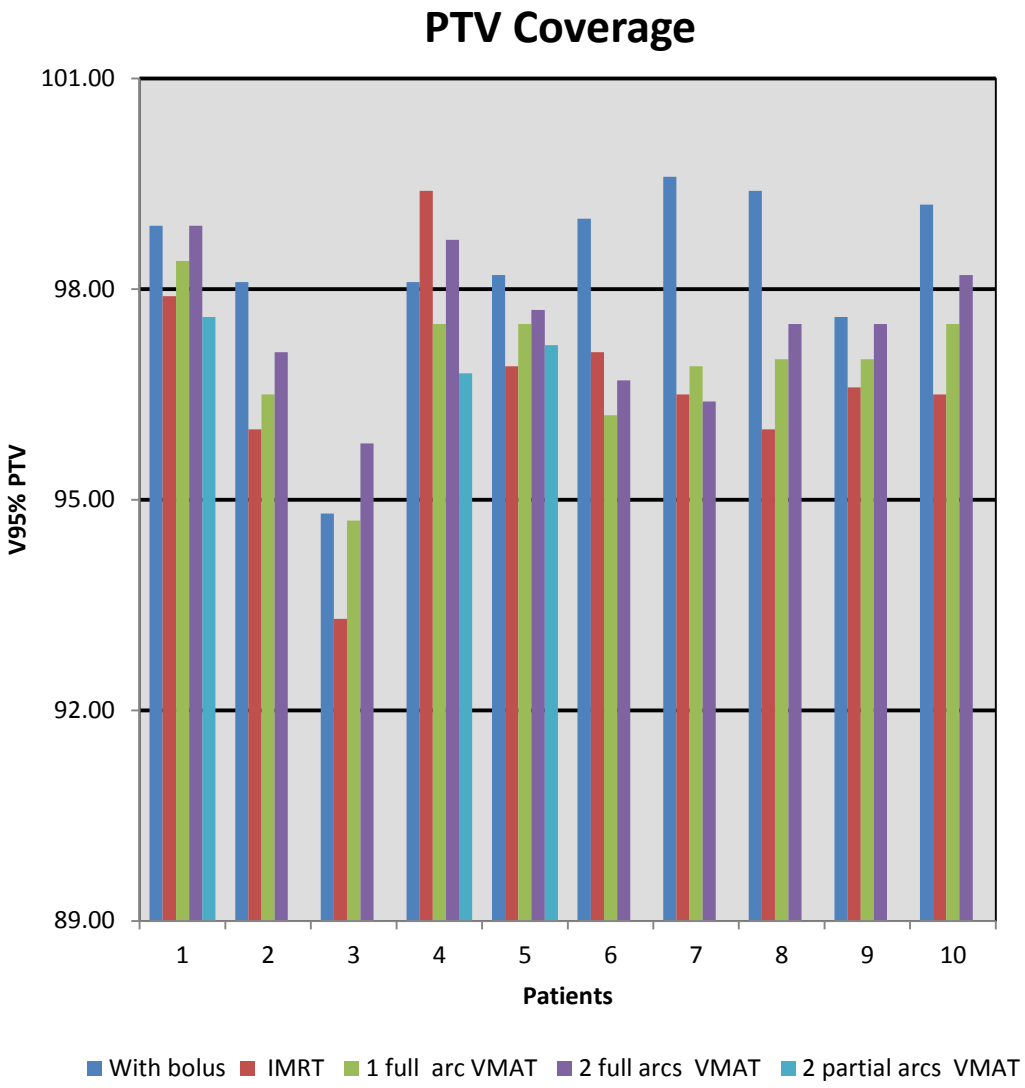

Figure 3.17: Comparison between the PTV coverage ($V_{95\%}$) in various trials for all case studies. As before, IMRT, '1 full arc VMAT', '2 full arcs VMAT' and ' 2 partial arc VMAT' are all 'no bolus' plans.

Among the no bolus plans, '2 arcs VMAT' plans gave better results in seven cases (Table 3.1) whilst IMRT plans were better in two cases. In one case, '1 arc VMAT' plan was slightly better than '2 arcs VMAT' plan.

Table 3.1: PTV coverage obtained in 'no bolus' treatment plans for ten patients. As indicated by the values in bold , '2 arcs VMAT' plans had better coverage in seven cases whilst '1 arc VMAT' was slightly better in one case. IMRT plans had greater PTV coverage in two cases. As the PTV coverage in '2 partial arcs VMAT' plans was lower than other no bolus VMAT plans, they were generated only for three patients.

Patients	IMRT	1 full arc VMAT	2 full arcs VMAT	2 partial arcs VMAT
1	97.90	98.40	**98.90**	97.60
2	96.00	96.50	**97.10**	
3	93.30	94.70	**95.80**	
4	**99.40**	97.50	98.70	96.80
5	96.90	97.50	**97.70**	97.20
6	**97.10**	96.20	96.70	
7	96.50	**96.90**	96.40	
8	96.00	97.00	**97.50**	
9	96.60	97.00	**97.50**	
10	96.50	97.50	**98.20**	

To analyse the impact of missing bolus on the skin ROI dose, the mean dose to the skin contour in each plan was normalised to the prescribed dose using Eq. 2. Fig. 3.18 shows the normalized skin ROI doses in treatment plans for the example patient given in Fig. 3.16. It is evident from the graph that the normalised skin ROI dose in the original plan with bolus is significantly greater than that in the new no bolus plans.

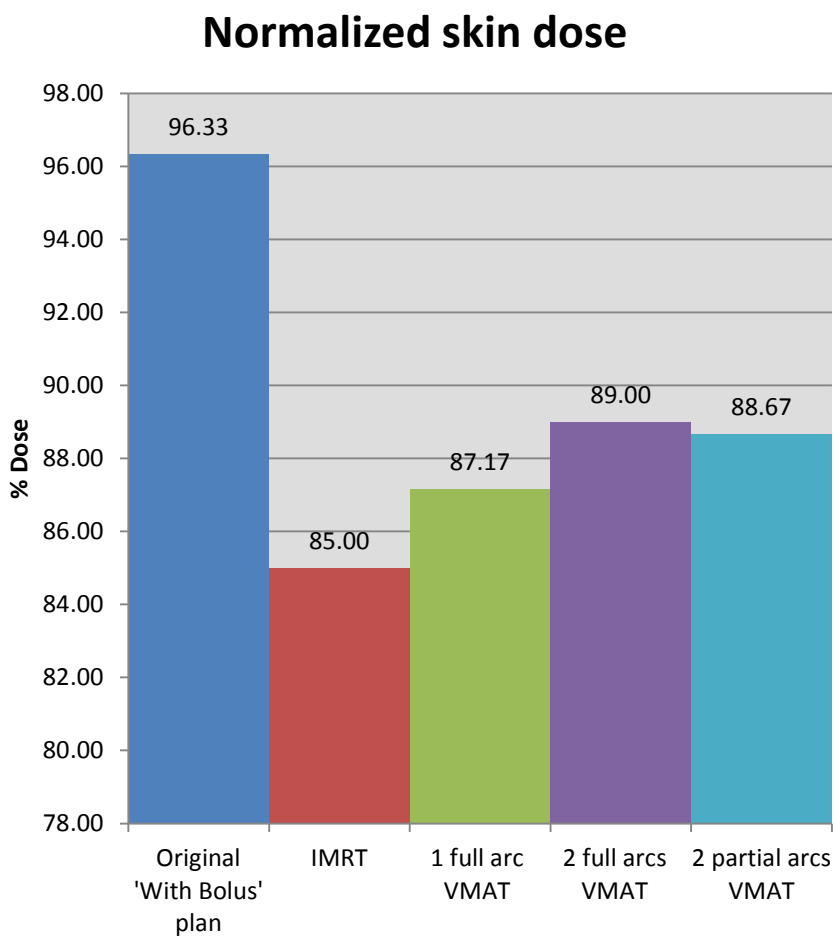

Figure 3.18: Mean skin ROI dose normalized to the prescribed dose in various trials for one patient.

Fig. 3.19 shows the normalized mean skin ROI doses to all patients in this study. The normalized mean skin ROI dose in all no bolus plans was significantly less than that in the original plans with bolus.

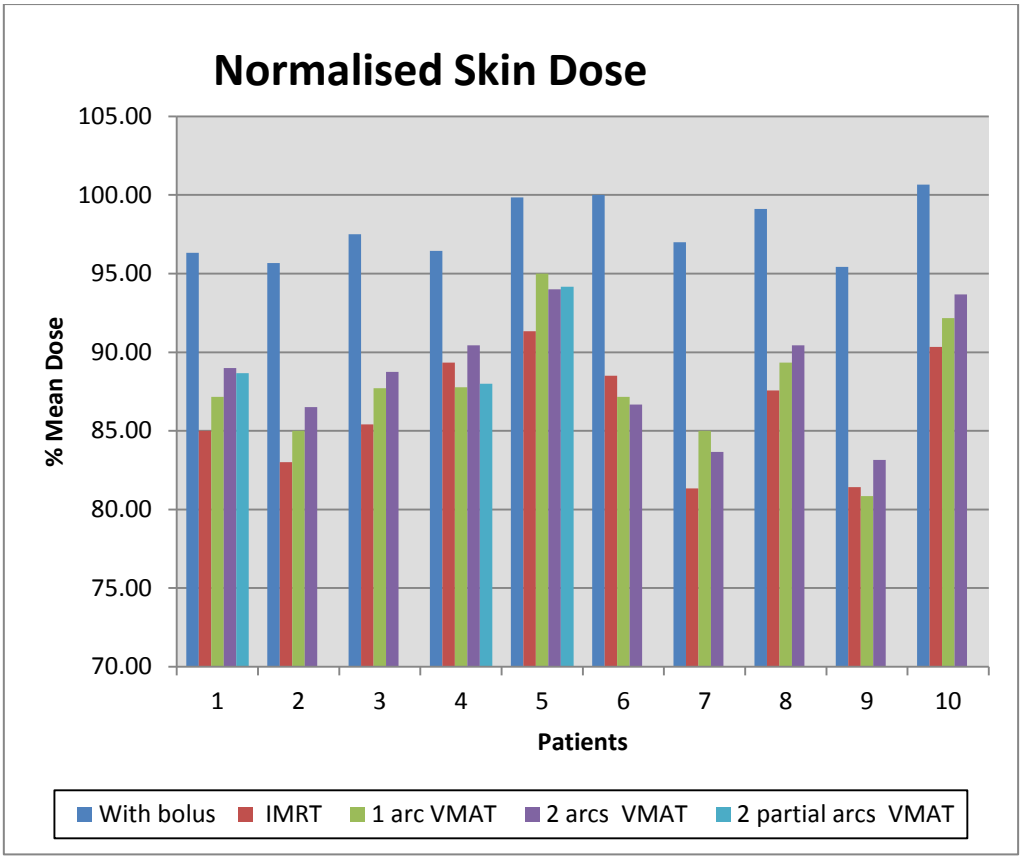

Figure 3.19: Normalized mean skin ROI doses in all plans for ten patients. The normalized mean skin ROI doses in 'non- bolus' plans were significantly less than that in the original plan with bolus.

Table 3.2 shows the mean normalized skin ROI dose for ten patients for each treatment planning technique. The skin ROI dose achievable without bolus was found to be significantly lower than that in the original plans with bolus. The average decrease in the skin ROI dose was 10.44%, 9.24%, and 8.48% in IMRT, '1 full arc VMAT', '2 full arcs VMAT' respectively.

Table 3.2: Mean normalized skin ROI doses in each treatment planning technique.

	Original plan with bolus	IMRT	1 arc VMAT	2 arcs VMAT
Mean normalized skin ROI dose	97.18±2.41%	86.74±5.82%	87.94±5.59%	88.70±5.16%

Normalised skin ROI doses in plans without bolus for individual patients are given in Table 3.3. '2 full arcs VMAT' plans had the highest normalised skin ROI dose in seven

cases whilst '1 full arc VMAT' gave better results in two cases . In one case, IMRT plan had a better outcome than other two techniques. However none of these techniques were able to produce a skin ROI dose that would have been clinically acceptable, as in the bolus plan.

Table 3.3: Normalised skin ROI doses in treatment plans without bolus for ten patients.

	Normalised skin ROI dose in plans without bolus (%)		
Patients	IMRT	1 full arc VMAT	2 full arcs VMAT
1	85.00	87.17	**89.00**
2	83.00	85.00	**86.50**
3	85.42	87.71	**88.75**
4	89.33	87.78	**90.44**
5	91.33	**95.00**	94.00
6	**88.50**	87.17	86.67
7	81.33	**85.00**	83.67
8	82.08	83.75	**84.79**
9	81.43	80.86	**83.14**
10	90.33	92.17	**93.67**

At ACH, the clinically acceptable global maximum dose (i.e. a maximum point dose anywhere in the plan) for IMRT and VMAT plans is 110% of the prescribed dose. This tolerance is adapted from the ICRU recommendation for IMRT and VMAT plans [16]. The global maximum dose in all no bolus plans in 'PTV coverage optimization' study was less than 110% of prescribed dose.

The results obtained in this section of treatment planning system (TPS) study showed that it was possible to achieve good PTV coverage without using bolus. However, the absence of bolus caused significant reduction in the skin ROI dose.

3.1.2 Optimising the skin ROI dose

In this section, the no bolus treatment plans were optimized to replicate the dose delivered *to the skin* in the original bolus plan and the overall impact on the dose

distribution was reported. In these plans, the skin ROI was considered as a 'cold spot' and the plans were optimized to deliver full doses to it.

Fig. 3.20 shows that in all no bolus plans the normalised skin ROI dose was greater than 97%. Thus it was possible to reproduce the dose delivered to the skin in the original plan. However, this approach had an adverse effect on the PTV coverage. For patient 3, the PTV coverage in the IMRT plan was comparable with the PTV coverage in the original plan with bolus. However, it was degraded in both VMAT plans without bolus. For patient 7, the PTV coverage in all plans without bolus was significantly smaller than the PTV coverage in original plan. Fig. 3.21 shows the PTV coverage in the original plan with bolus and a new plan without bolus for patient 3. Whilst the PTV in original plan with bolus gets at least 95% of the prescribed dose, a significant part of the PTV is underdosed in the new no bolus plan.

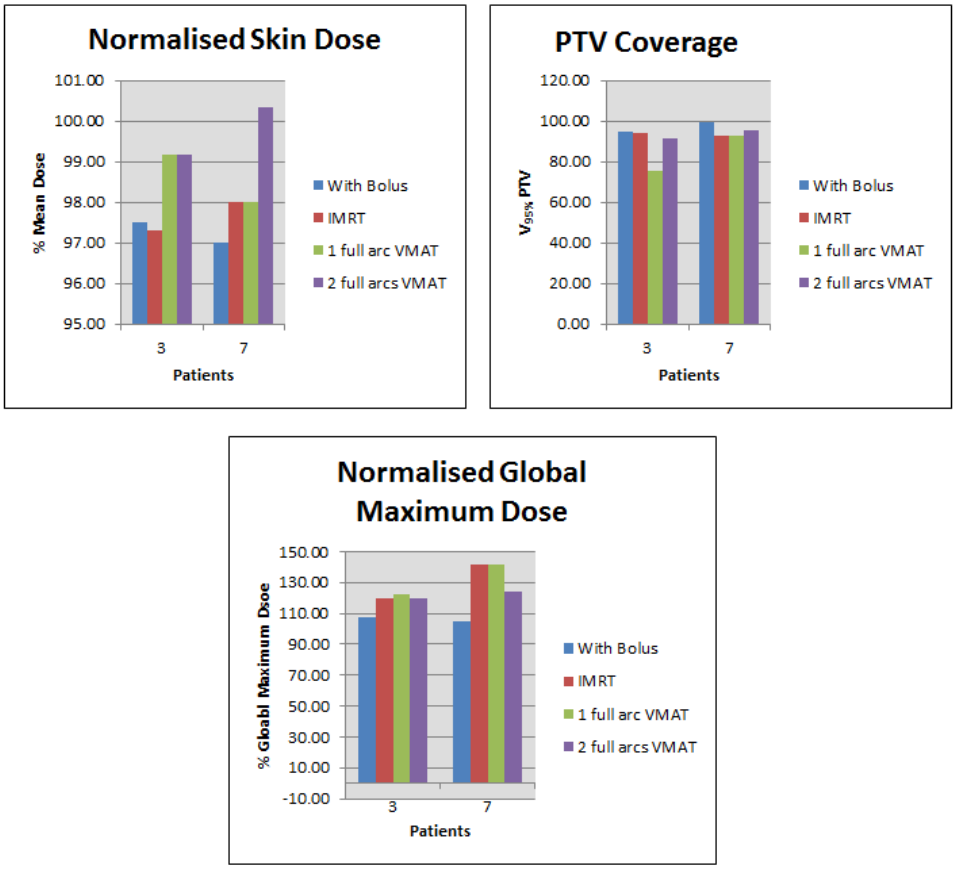

Figure 3.20: The effect of optimizing dose to the skin ROI on normalised skin ROI dose, PTV coverage and global maximum dose in no bolus treatment plans for two patients.

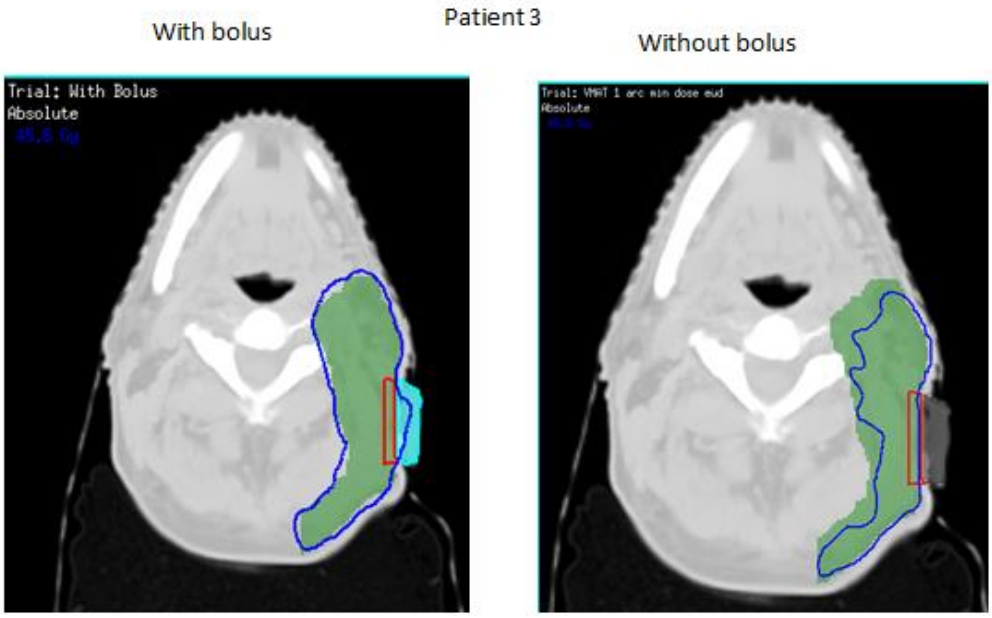

Figure 3.21: Comparison between PTV coverage in the original plan with bolus and the new 1 full arcs VMAT plan without bolus for Patient 3. 95% isodose line (blue) conforms well to the PTV (green colourwash) in original plan with bolus. However, it does not conform tightly to the PTV in the new bolus plan without bolus.

The skin ROI was in the build-up region of megavoltage photon beam which is a low dose region (as discussed in section 1.1.3). When the plan was optimized to deliver high doses in this region, the optimizing algorithm attempted to increase the dose by creating intensity peaks in fluence maps [57]. This caused hot spots in the plans outside the target volume. Hot spots are volumes of tissues that receive doses greater than the prescribed dose. If the hot spots are in normal tissues, they can cause severe damage. Hence hot spots outside the target volumes are undesirable [16]. As seen in Fig. 3.20, the global maximum doses in the new no bolus plans were above tolerance limit (110%). Hence, these plans would not be clinically acceptable.

The treatment planning needs a considerable amount of time and resources. In the 'skin ROI dose optimization' study, three no bolus plans were generated per patient. All these plans were suboptimal (inadequate PTV coverage and hotspots in normal tissues) and would not be clinically accepted. Hence, this method was not attempted for other patients.

3. 2 Dosimetry

3.2.1 Film calibration and uncertainty analysis

EBT3 films were calibrated for a dose range of 0 - 600 cGy. Mean pixel values obtained using the ImageJ software were converted into optical density (OD) using Eq. 3. The netOD values were obtained by subtracting the OD of an unexposed (background) film. The calibration curve was fitted with a third order polynomial (R^2= 0.99961) (Fig.3.22) [66].

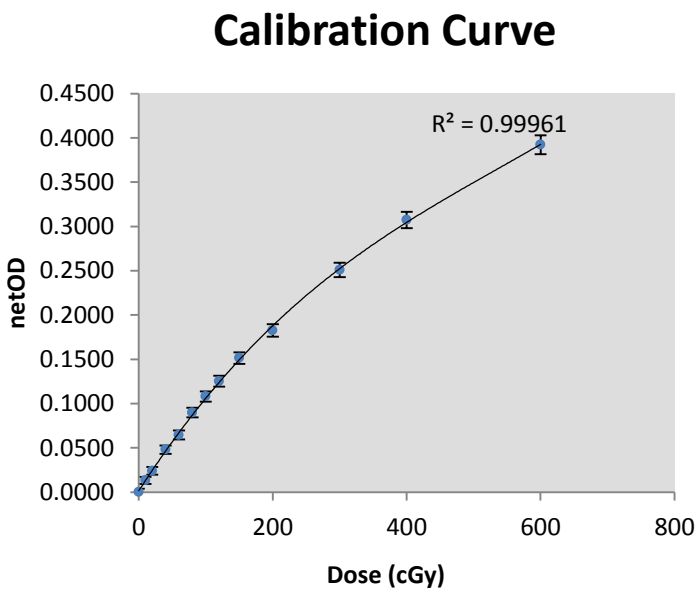

Figure 3.22: Calibration curve of EBT3 film for 6 MV photon beam.

The relative uncertainties in the doses measured by film are given Table 3.4.

Table 3.4: Uncertainty determination for EBT3 film

Source of uncertainty	Relative uncertainty (%)
Film Uniformity	±0.84
Inter-sheet variation	±1.38
Single film scanner reading reproducibility	±0.48

The combined relative uncertainty was calculated by a quadrature sum of the above uncertainties (assumed as independent) as follows:

$$Combined\ uncertainty = \sqrt{0.84^2 + 1.38^2 + 0.48^2} = 1.69\% \qquad \text{Eq. 6}$$

3.2.2 Surface dose measurement with a parallel plate chamber and EBT3 films

Doses at a range of depths from the surface (0 mm) to 15mm were measured with a PPC40 parallel plate ionization chamber and were normalised to 100% at the depth of maximum dose (15mm). The percentage depth dose (PDD) data thus obtained is shown in Table 3.5. The effective point of measurement for a PPC40 is 1 mm below the entrance window. The depths were corrected accordingly.

Table 3.5: Percentage depth dose in build-up region measured with a PPC40 ionization chamber

Corrected Depth (mm)	PDD (%)
1.00	50.4±0.12
4.00	82.0±0.13
6.00	90.5±0.19
8.00	95.9±0.19
11.00	99.3±0.18
14.00	99.9±0.20
15.00	100.0±0.18

Measured PDD values were corrected for over-response in the build-up region using Eq. 5 and were plotted against depth as shown in Fig. 3.23. A 6^{th} degree polynomial (R^2 =1) was fitted to the corrected data and the surface dose was obtained by extrapolating the curve to a depth of 0. The percentage surface dose was found to be 17.6%.

Bilge *et al*. [35] measured surface dose with a Markus parallel-plate ionization chamber. They found that the surface dose for a 6 MV photon beam with a field size of 10 × 10 cm^2 was 15.0%. Jong and colleagues measured surface dose with a Markus chamber and the result for a 10 x 10 cm^2 6 MV photon beam was 15.83±0.03% [67]. In another study, the surface dose measured with an Attix parallel-plate ionization chamber was 18.95% [68]. Akbas *et al*. [36] showed that the surface dose measured with a Markus chamber was 16.61%. In a Monte Carlo study, the surface dose for 10 x 10 cm^2 6 MV photon beam was 16.45% [69] . In the present study, the surface dose measured with a PPC parallel-plate chamber was 17.6%. This result shows coherency with other studies.

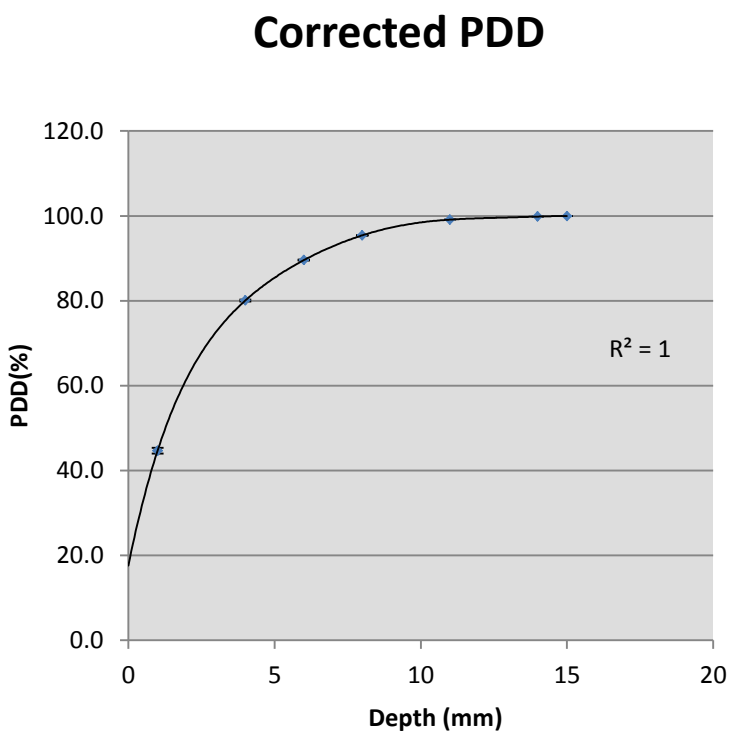

Figure 3.23: Corrected PDD. Percentage depth dose data obtained with a PPC40 chamber were corrected for over-response in the build-up region using Gerbi's correction factors.

Percentage surface dose measured with EBT3 film was found to be 20.9 ± 2.4%. This value was in close agreement with the surface dose measured by Akbas *et al*. In their study, percentage surface dose measured with EBT3 film was 20.4% [36].

The results obtained in this study showed that surface dose may be overestimated by 3.3% with EBT3 Gafchromic film measurement with respect to the PPC40 ionization chamber for 6 MV photons. This is comparable with the results of the investigation by Bilge *et al.* [35]. In their study, the surface doses measured with EBT film were 5% higher than the parallel plate ionisation chamber measurements for a 6 MV beam.

The surface dose is defined as the dose deposited within an infinitesimally small mass of matter at the surface of the phantom/patient. However, the radiation detectors do not have an infinitesimally small sensitive volume. Hence, surface dose measurements are fundamentally difficult. For practical reasons, the dose measured at the effective point of measurement of the detector at depth of 0 mm is considered as the surface dose. Even though the detectors may have a very shallow

effective point of measurement, the measured dose is not strictly the surface dose. This causes the discrepancy between the surface doses measured by different detectors [70, 36]. PPC40 chamber used in this study has an effective point of measurement at 1 mm below the front window and the surface dose was obtained by extrapolating the PDD curve [71]. For the EBT3 film, it was assumed to be at the surface of the film [72]. This may have resulted in the discrepancy between the two measurements.

3.2.3 Surface dose comparison

3.2.3.1 Point doses

Point doses were measured using the measurement set-up described in section 2.3.5.4. Measured point doses were in good agreement with point doses predicted by Pinnacle^3 (Table 3.6). For all plans, the dose difference was within ± 3% which is well within the accepted clinical tolerance based on ICRU recommendations [73]. This verified the accuracy of treatment delivery.

Table 3.6: Comparison between measured dose and dose predicted by Pinnacle^3

	Point Dose measurement (Gy)		
Patient Plans	Measured Dose (Film)	Pinnacle^3	Dose Difference
Patient1_NoBolus	1.87±0.01	1.88±0.06	0.53%
Patient1_Bolus	2.00 ±0.01	2.01±0.06	0.50%
Patient9_NoBolus	1.96 ± 0.01	2.01±0.06	2.49%
Patient9_Bolus	1.97±0.01	1.92±0.06	-2.60%

3.2.3.2 Surface dose

Surface doses in treatment plans were measured using the measurement set-up described in section 2.3.5.4. The surface dose measured with EBT3 film and the surface doses obtained from Pinnacle^3 for both patients is given in Table 3.7. In the

plans without bolus, Pinnacle^3 overestimated the surface dose compared to film measurements for Patient 1 and Patient 9 by 19.6% and 31.1% respectively.

Table 3.7: Comparison between surface doses measured with EBT3 films and calculated by Pinnacle^3

Patient Plans	Surface dose measured by film dosimetry (Gy)	Surface dose calculated by Pinnacle^3(Gy)
Patient1_NonBolus	1.27±0.02	1.58±0.10
Patient1_WithBolus	2.08±0.04	2.02±0.11
Patient9_NonBolus	1.13±0.02	1.64±0.04
Patient9_WithBolus	1.91±0.03	1.91±0.15

Roland *et al*. [74] found that Pinnacle^3 overestimated the average surface dose by 15% compared to the surface doses measured with EBT films and TLD. Chung and colleagues measured the surface dose with Gafchromic film HS and compared it with surface dose calculated in Pinnacle^3. They found significant discrepancies (~7.4% to 18.5%) between the measured dose and calculated dose near surface [30]. The surface dose in the no bolus plan for Patient 1 (19.6%) shows good agreement with these results. However, for Patient 9, the discrepancy is large (31.1%). This large discrepancy could be due to the difficulty in matching the exact location of the film on the phantom during delivery and the corresponding location on the scanned phantom in Pinnacle^3 as the setup for Patient 9 was more complex. Whilst great care was taken to reproduce the setup in TPS during the delivery, there could have been an error in placing the film on planned position.

Pinnacle^3 significantly overestimated the surface doses the new no bolus plans. The dose in the build-up region depends upon different factors such as the primary photon beam, backscattered radiation from patient, and contamination electrons originating in the linear accelerator head as well as in the air volume between the linear accelerator head and patient. Modelling the source of build-up dose is very complex. Hence, an electron contamination is normally added to the dose distribution after the photon dose is calculated in model-based calculation algorithm such as Collapsed Cone Convolution Superposition (CCCS). Accuracy of the dose in

the build-up region is greatly affected by the accuracy of the electron contamination model in different irradiation conditions. As stated in section 1.2.1, electron contamination modelling in Pinnacle^3 is simplified by assuming that the electron contamination does not depend on the source-to-surface distance or on other beam modifiers. This leads to the discrepancy in the surface dose predicted by Pinnacle^3 and measured surface dose [29, 30].

For the original plans with bolus, the discrepancy between the measured dose on the surface of the phantom and Pinnacle^3 dose was ±3.1%, i.e. Pinnacle was able to accurately predict phantom surface dose under bolus. In the original plans, a bolus of thickness 7 mm was placed on the film. In other words, the film was at a depth of 7 mm. Chung et al. [30] demonstrated that for shallow targets (~5 mm) the difference in Pinnacle^3 dose and measured dose was ±5.6%. The results in this study were consistent with this finding.

4. Conclusion

In the present study, IMRT and VMAT techniques were used for head and neck planning and surface doses in the original plans with bolus were compared with newly developed no bolus plans. In the original plan with bolus, the clinical objectives were to achieve optimal PTV coverage, doses to OARs within their tolerance limit, maximum dose in the overall plan less than 110%, and full dose to scar tissues. In the treatment planning study, attempts were made to generate a no bolus plan which would have comparable PTV coverage and dose to scar tissues as high as the original plan with bolus. To achieve this, two different approaches – 'optimizing PTV coverage' and 'optimizing skin dose' - were tried. The first method produced no bolus plans with PTV $V_{95\%} \geq 95\%$. In these plans, OAR doses were comparable with those in the original plans and there were no hot spots outside the target volume. Hence, these plans achieved the first three clinical goals. However, they could not achieve the required dose to scar tissues in these. On the other hand, in the 'Skin dose optimization' method, it was possible to give full doses to scar tissues. However, these plans produced sub-optimal dose distributions (PTV $V_{95\%} < 95\%$ and hotspots in normal tissues) which would not be clinically acceptable.

Surface doses predicted by Pinnacle[3] were verified by film dosimetry. Surface dose measured with EBT3 film was validated by the surface dose measured with a parallel plate chamber. Surface doses measured with the parallel plate chamber PPC40 and EBT3 film were 17.6% and 20.9% respectively. They were in good agreement. Surface dose in the original plans with bolus and the new bolus plans without bolus were verified by delivering plans to the cylindrical phantom. Measured surface dose in the original plan with bolus was in good agreement with the dose predicted by Pinnacle[3]. However, there was considerable discrepancy in measured and predicted surface doses for the no bolus plans. Pinnacle[3] overestimated the surface doses in the no bolus plans.

If the goal is to adequately treat the scar tissue whilst maintaining a good quality dose distribution within the target, this study demonstrates that bolus is a necessary component of the treatment delivery process. The scope of this study could be

expanded by increasing the sample size and grouping similar cases. This could help develop a class solution for these cases.

References

[1] K. Plichta and H. B. Mackley, “Radiotherapy for cutaneous malignancies of the head and neck,” *Operative techniques in otolaryngology,* vol. 24, no. 1, pp. 59-62, 2013.

[2] R. Basker, K. A. Lee, R. Yeo and K.-W. Yeoh, “Cancer and Radiation Therapy : Current Advances and Future Directions,” *International Journal of Medical Sciences,* vol. 9, no. 3, pp. 193-199, 2012.

[3] M. Joiner and A. v. d. Kogal, Eds., Basic Clinical Radiobiology, 4 ed., London: Hodder Arnold, 2009.

[4] B. Vujosevic and B. Bokorov, “Radiotherapy: past and present,” *Archive of oncology,* vol. 18, no. 4, pp. 140-142, 2010.

[5] E. B. Podgorsak, “External photon beams: physical aspects,” in *Radiation Oncology Physics: A handbook for teachers and students*, E. B. Podgorsak, Ed., Vienna, International Atomic Energy Agency, 2005.

[6] J. Talbot, *A patient position guidance system in radiotherapy using augumented reality,* MSc thesis,University of Canterbury, 2009.

[7] “The University of Western Australia School of Physics,” 2016. [Online]. Available: http://www.physics.uwa.edu.au/research/medical-radiation/projects/vmat. [Accessed 8 April 2016].

[8] H. E. Johns and J. R. Cummingham, The Physcis of Radiology, 4 ed., Springfield, illinois: Charles C Thomas, 1983.

[9] J. P. Seuntjens, W. Strydom and K. R. Shortt, “Dosimetric Principles, Quntities and Units,” in *Radiation Oncology Physics: A handbook for teachers and students*, E. B. Podgorsak, Ed., Vienna, IAEA, 2005, pp. 45-70.

[10] K. Cooke, “X-ray interaction with matter,” in *Practical Radiotherapy Physcis and Equipments*, 2 ed., P. Cherry and A. M. Duxbury, Eds., Sussex, Wiley-Blackwell, 2009, pp. 36-47.

[11] M. K. Bucci, A. Bevan and M. Roach III, “Advances on Radiation Therapy: Conventional to 3D, to IMRT, to 4D, and beyond,” *CA Cancer Journal for Clinicians,* vol. 55, no. 2, pp. 117-134, 2005.

[12] A. R. Smith, Ed., Radiation Therapy Physics, Springer , 2013.

[13] S. Huq and P. Mayles, “IAEA-TECDOC-1588 Transition from 2-D Radiotherapy to 3-D Conformal and Intensity Modulated Radiotherapy,” International Atomic Energy Agency, Vienna, 2008.

[14] K. K. Ang and A. S. Garden, Radiotherapy for Head and Neck Cancers - Indications and Techniques, 3 ed., Lippincott Williams & Wilkins, 2006.

[15] N. G. Burnet, S. J. Thomas, K. E. Burton and S. J. Jefferies, “Defining the tumour and target volumes for radiotherapy,” *Cancer Imaging,* vol. 4, no. 2, pp. 153-161, 2004.

[16] V. Gregoire, T. R. Mackie, W. De Neve, M. Gospodarowicz, J. A. Purdy, M. van Herk and A. Niemierko, “ICRU Report No. 83 Prescribing, recording, and reporting photon-beam intensity-modulated radiation therapy(IMR),” Oxford University Press, Oxford, 2010.

[17] A. J. Mundt and J. C. Roeske, Intensity modulated radiation therapy- A clinical perspective, Hamilton: BC Decker Inc, 2005.

[18] W. Schlegel, T. Bortfeld and A.-L. Grous, New Technologies in Radiation Oncology, Berlin: Springer , 2006.

[19] S. Webb, The physics of conformal radiotherpy - Advances in technology, Bristol: Institute of Physics Publishing, 1997.

[20] L. Shao, “A survey of beam intensity optimizaiton in IMRT,” in *Proceedings of the 40th Annual Conference of the Operational Society of New Zealand*, Wellington, 2005.

[21] W. F. Verbakel, J. P. Cuijpers, D. Hoffmans, M. Bieker, B. J. Slotman and S. Senan, “Volumetric intensity-modulated arc therapy vs conventional IMRT in head-and-neck cancer: a comparative planning and dosimetric study,” *International Journal of Radiation Oncology Biology Physics,* vol. 74, no. 1, pp. 252-259, 2009.

[22] K. Otto, “Volumetric modulated arc therapy:IMRT in a single arc,” *Medical Physics,* vol. 35, no. 1, pp. 310-317, 2008.

[23] F. Peng, “Optimization methods for volumetric modulated arc therapy and radiation therapy under uncertainty,” University of Michigen, 2013.

[24] A. Argiris, M. V. Karamouzis, D. Raben and R. L. Ferris, “Head and neck cancer,” *Lancet,* vol. 371, pp. 1695-1709, 2008.

[25] M. k. Bucci, A. Bevan and M. Roach III, “Advances in Radiation Therapy: Conventional to 3D, to IMRT, to 4D, and beyond,” *CA Cancer Journal for Clinicians,* vol. 55, no. 2, pp. 117-134, 2005.

[26] U. Parvathaneni, G. E. Laramore and J. J. Liao, “Technical Advances and Pitfalls in Head and Neck Radiotherapy,” *Journal of Oncology,* vol. 2012, 2012.

[27] Auj-e-Taqaddas, Investigation of VMAT Algorithm and Dosimetry, Bloomington: AuthorHouse, 2014.

[28] T. McNutt, “Dose Calculations Collapsed Cone Convolution Superposition and Delta Pixel Beam [White Paper],” Royal Phillips Electronics, Eindhoven, 2007.

[29] G. Starkschall, R. E. Steadham, R. A. Popple, S. Ahmad and I. I. Rosen, “Beam-commissioning methodology for a three-dimensional convolution/superposition photon dose algorithm,” *Journal of Applied Clinical Medical Physics,* vol. 1, no. 1, 2000.

[30] H. Chung, H. Jin, J. F. Dempsey, C. liu, J. Palta, T.-s. Suh and S. Kim, “Evaluation of surface and build-up region dose for intensity-modulated radiation therapy in head and neck cancer,” *Medical Physics,* vol. 32, no. 8, pp. 2682-2689, August 2005.

[31] A. D. Guerra, Ionizing radiation detectors for medical imaging, Singapore: World Scientific Publishing Co. Pte. LTD, 2004.

[32] *Detectors for Relative and Absolute Dosimetry - Ionization Chambers and Diod detectors,* IBA.

[33] F. M. Khan, The physics of radiation therapy, 4 ed., Philadelphia: Lippincott Williams & Wilkins, 2010.

[34] B. J. Gerbi and F. M. Khan, “Measurement of dose in the buildup region using fixed-seperation plane-parallel ionization chambers,” *Medical Physics,* Vols. 17-26, 1990.

[35] H. Bilge, A. Cakir, M. Okutan and H. Acar, “Surface dose measurements wth Gafchromic EBT film for 6 and 18 MV photon beams,” *Physica Medica,* vol. 25, pp. 101-104, 2009.

[36] U. Akbas, N. D. Kesen, C. Koksal and H. Bilge, “Surface and buildup region dose measurements with Markus parallel-plate ionization chamber, Gafchromic EBT3 film and MOSFET detector for high energy photon beams,” *arXiv:1601.03570v1[physics.ins-det],* January 2016.

[37] K. H. Looe, D. Harder and B. Poppe, “Experimental determination of the effective point of measurement for various detectors used in photon and electron beam dosimetry,” *Physcis in Medincine and Biology,* vol. 56, pp. 4267-4290, 2011.

[38] “IAEA TRS-398 Absorbed dose determination in External Beam Radiotherapy: An international code of practice for Dosimetry based on Standards of Absorbed Dose to water,” International Atomic Energy Agency, Vienna, 2006.

[39] B. Currie, *Calibration of Electron and Photon Beams,* University of Canterbury, 2013.

[40] M. J. Williams and P. E. Metcalfe, “Radiochromic film dosimetry and its applicaitons in radiotherapy,” in *Concepts and trends in medical radiation dosimetry: Proceedings of*

the SSD Summer School, Wollongong, 2011.

[41] Y. Shimohigashi, F. Araki, M. Maruyama, Y. Nakaugchi, Y. Kuwahara, S. Kuwahara, N. Nagasue and Y. Kai, "Evaluation of a single-scan protocol for radiochromic film dosimetry," *Journal of Applied Clinical Medical Physics,* vol. 16, no. 2, 2015.

[42] V. Rudat, A. Nour, A. A. Alaradi, A. Mohamed and S. Altuwaijri, "In vivo surface dose measurement using Gafchromic film dosimetry in breast cancer radiotherapy: comparison of 7-field IMRT, tangential IMRT and tangential 3D-CRT," *Radiation Oncology,* vol. 9, 2014.

[43] S. Reinhardt, M. Hilbrand and W. Assmann, "Comparison of Gafchromic EBT2 and EBT3 films for clinical photon and proton beams," *Medical Physics,* vol. 39, no. 8, pp. 5257-5262, August 2012.

[44] V. C. Borca, M. Pasquino, G. Russo, P. Grosso, D. Cante, P. Sciacero, G. Girelli, M. R. La Porta and S. Tofani, "Dosimetry characterization and use of GAFCHROMIC EBT3 film for IMRT dose verification," *Journal of Applied Clinical Medical Physics,* vol. 14, no. 2, pp. 158-171, 2013.

[45] G. Massillon-JL, S.-T. Chiu-Tsao, I. Domingo-Munoz and M. F. Chan, "Energy Dependence of the New Gafchromic EBT3 film: Dose Response Curves for 50 kV, 6 and 15 MV X-Ray Beams," *International Journal of Medical Physics, Clinical Engineering and Radiation Oncology,* vol. 1, pp. 60-65, 2012.

[46] S. Devic, "Radiochromic film dosimetry: Past, present, and future," *Physica Medica,* vol. 27, pp. 122-134, 2011.

[47] J. Van Dam and G. Marinello, Methods for in vivo dosimetry in external radiotherapy, 2 ed., Brussels: ESTRO, 2006.

[48] V. Vyas, L. Palmer, R. Mudge, R. Jiang, A. Fleck, B. Schaly, E. Osei and P. Charland, "On bolus for megavoltage photon and electron radiation therapy," *Medical Dosimetry,* vol. 38, no. 3, pp. 268-273, 2013.

[49] N. Lee, D. R. Puri, A. I. Blanco and K. Chao, "Intensity-modulated radiation therapy in head and neck cancers: An update," *Head & Neck,* vol. 29, no. 4, pp. 387-400, April 2007.

[50] N. Dogan and G. P. Glasgow, "Surface and build-up region dosimetry for obliquely incident intensity modulated radiotherapy 6 MV x rays," *Medical Physics,* vol. 30, no. 12, pp. 3091-3096, December 2003.

[51] S. Yokoyama, P. L. Roberson, D. W. Litzenberg, J. M. Moran and B. A. Fraass, "Surface buildup dose dependence on photon field delivery techniques for IMRT," *Journal of Applied Clinical Medical Physics,* vol. 5, no. 2, pp. 71-81, 2004.

[52] J. C. Chow, G. N. Grigorov and R. B. Barnett, “Study on surface dose generated in prostate intensity-modulated radiation therapy treatment,” *Medical Dosimetry,* vol. 31, no. 4, pp. 249-58, 2006.

[53] P. D. Higgins, E. y. Han, J. L. Yuan, S. Hui and C. K. Lee, “Evaluation of surface dose and superficial dose for head and neck treatments using conventional or intensity-modulated technqiues,” *Physics in Medicine and Biology,* vol. 52, pp. 1135-1146, 2007.

[54] E. P. Saibishkumar, M. A. MacKenzie, D. Severin, A. Mihai, J. Hanson, H. Daly, G. Fallone, M. B. Parliament and B. S. Abdulkarim, “Skin-sparing radiation using intensity modulated radiotherapy after conservative surgery in early-stage breast cancer: a planning study,” *International Journal of Radiation Oncology Biology Physics,* vol. 70, no. 2, pp. 485-491, 2008.

[55] M. J. Buston, T. Cheung, P. Yu and P. Metcalfe, “Effects of skin dose from unwanted air gaps under bolus in photon beam radiotherapy,” *Radiation Measurements,* vol. 32, pp. 201-204, 2000.

[56] A. Sibatain, A. Morgan and N. MacDougall, Eds., Radiotherapy in Practice Physics for Clinical Oncology, Oxford: Oxford University Press, 2012.

[57] W. De Neve, Y. Wu and G. Ezzell, “Practical IMRT Planning,” in *Image-Guided IMRT*, T. Bortfeld, Schmidt-Ullrich, W. De Neve and D. E. Wazer, Eds., Berlin, Springer, 2006, pp. 46-60.

[58] G. S. Sim, J. Wong and K. H. Ng, “The use of radiochromic EBT2 film for the quality assurace and dosimetric verification of 3D conformal radiotherapy using Microtek ScanMaker 9800XL flatbed scanner,” *Journal of Applied Clinical Medical Physics,* vol. 14, no. 4, pp. 85-95, July 2013.

[59] R. Dreindl, D. Georg and M. Stock, “Radiochromic film dosimetry: Consideration on precision and accuracy for EBT2 and EBT3 type films,” *Z. Medical Physics,* vol. 24, pp. 153-163, 2014.

[60] J. Sorriaux, A. Kacperek, S. Rossomme, J. A. Lee, D. Bertrand, S. Vynckier and E. Sterpin, “Evaluation of Gafchromic EBT3 films characteristics in therapy photon, electron and proton beams,” *Physica Medica: European Journal of Medical Physics,* vol. 29, no. 6, pp. 599-606, 2013.

[61] P. Andreo, P. R. Almond, O. Mattsson, A. E. Nahum and M. Roos, “IAEA Code of Practice for plane-parallel ionization chambers TRS-381,” International Atomic Energy Agency, Vienna, 1995.

[62] *Technical Bulletin 08-11 ArcCheck - CT Images,* Melbourne, Florida: Sun Nuclear Corporation, 2011.

[63] *ArcCheck Refernce Guide,* Melbourne: Sun Nuclear Corporation, 2013.

[64] S. Rana, “Intensity modulated radiation therapy versus volumetric intensity modulated arc therapy,” *Journal of Medical Radiation Science,* vol. 60, no. 3, pp. 81-83, 2013.

[65] M. Teoh, C. H. Clark, K. Wood , S. Whitaker and A. Nisbet, “volumetric modulated arc therapy: a review of current literature and clinical use in practice,” *The British Journal of Radiology,* vol. 84, no. 1007, pp. 967-996, 2011.

[66] G. S. Sim, J. Wong and K. Ng, “The use of radiochromic EBT2 film for the quality assurance and dosimetric verificaiton of 3D conformal radiotherapy using Mircroteck ScanMaker 9800XL flatbed scanner,” *Journal of Applied Clinical Medical Physics,* vol. 14, no. 4, 2013.

[67] W. L. Jong, J. Wong, N. M. Ung, K. H. Ng, G. F. Ho, D. L. Cutajar and A. B. Rosenfield, “Characterization of MOSkin detector for in vivo skin dose measurement during megavoltage radiotherapy,” *Journal of Applied Clinical Medical Physics,* vol. 15, no. 5, pp. 120-132, 2014.

[68] Z.-y. Qi, D. Xiao-Wu, S.-m. Huang, L. Zhang, Z.-C. He, X. A. Li, I. Kwan, M. Lerch, D. Cutajar, P. Metcalfe and A. Rosenfeld, “In vivo verification of superficial dose for head and neck treatments using intensity-modulated techniques,” *Medical Physics,* vol. 36, no. 1, pp. 59-70, 2009.

[69] L. Apipunyasopon, S. Srisatit and N. Phaisangittisakul, “An investigation of the depth dose in the build-up region, and surface dose for a 6-MV therapeutic photon beam: Monte Carlo simulation and measurements,” *Journal of Radiation Research,* vol. 54, no. 2, pp. 374-382, 2013.

[70] S. Devic, J. Seuntjens, W. Abdel-Rahman, M. Evans, M. Olivares, E. B. Podgorsk, T. Vuong and C. G. Soares, “Accurate skin dose measurements using radiochromic film in clinical applications,” *Medical Physics,* vol. 33, no. 4, pp. 1116-1124, 2006.

[71] *PPC40 Ionization Chamber User's Guide,* Schwarzenbruck: IBA , 2013.

[72] T. A. Brown and K. R. Hogstrom, “Dose-response curve of EBT, EBT2, and EBT3 radiochromic films to synchrotron-produced monochromic x-ray beams,” *Medical Physics,* vol. 39, no. 12, pp. 7412-7417, December 2012.

[73] “ICRU 24: Determination of Absorbed Dose in a Patient Irradiated by Beams of X or gamma rays in Radiotherapy Procedures,” ICRU, Washington, D. C., 1976.

[74] T. F. Roland, S. Stathakis, R. Ramer and N. Papanikolaou, “Measurement and comparison of skin dose for prostate and head-and-neck patients treated on various IMRT delivery systems,” *Applied Radiation and Isotopes,* vol. 66, no. 12, pp. 1844-1849, December 2008.

[75] H. Bilge, N. Ozbek, M. Okutan, A. Cakir and H. Acar, “Surface dose and build-up region measurements with wedge filters for 6 and 18 MV photon beams,” *Japnese Journal of Radiology,* vol. 28, pp. 110-116, 2010.

[76] L. Richley, A. C. John, H. Coomber and S. Fletcher, “Evaluation and optimization of the new EBT2 radiochromic film dosimetry system for patient dose verification in radiotherapy,” *Physics in Medicine and Biology,* vol. 55, pp. 2601-2617, 14 April 2010.

[77] R. Dreindl, D. Georg and M. Stock, “Radiochromic film dosimetry: Consideration on precision and accuracy for EBT2 and EBT3 type film,” *Journal of Medical Physics ,* vol. 24, pp. 153-163, 2014.

[78] J. Sorriaux, A. kacperek, S. Rossomme, J. A. Lee, D. Bertrand, S. Vynckier and E. Sterpin, “Evaluation of Gafchromic EBT3 films characteristics in therapy photon, electron and proton beams,” *Physica,* pp. 1-10, 2012.

[79] T. Brown, K. Hogstrom, D. Alvarez, K. L. Mathews II, K. ham and J. Dugas, “Dose-response curve of EBT, EBT2, and EBT3 radiochromic films to synchrotron-produced monochromatic x-ray beams,” *Medical Physics,* vol. 39, no. 12, pp. 7412-7417, 2012.

[80] M. Martisikova, B. Achermann and O. Jakel, “Analysis of uncertainties in Gafchromic EBT film dosimetry of photon beams,” *Physics in Medicine and Biology,* vol. 53, pp. 7013-7027, 2008.

[81] S. Davic, J. Seuntjens, W. Abdel-Rahman, M. Evans, M. Olivares and E. B. Podgorsak, “Accurate skin dose measurements using radiochromic film in clinical applications,” *Medical Physics,* vol. 33, no. 4, pp. 1116-1123, 2006.

[82] S.-T. Chiu-Tsao and M. F. Chan, “Evaluaton of two-dimensional bolus effect of immobilization/support devices on skin doses - A radiochromic EBT film dosimetry study in phantom,” *Medical Physics,* vol. 37, no. 7, pp. 3611-3620, July 2010.

[83] N. Lee, D. R. Puri, A. I. Blanco and K. Chao, “Intensity-modulated radiation therapy in head and neck cancer: an update,” *Head and neck,* vol. 29, no. 4, pp. 387-400, April 2007.

[84] N. Dogan and G. P. Glasgow, “Surface and build-up region dosimetry for obliquely incident intensity modulated radiotherapy 6 MV x rays,” *Medical Physics,* vol. 30, no. 12, pp. 3091-3096, December 2003.

[85] P. Andreo, D. T. Burns, K. Hohlfeld, M. S. Huq, T. Kanai, F. Laitano, V. G. Smyth and S. Vynckier, “IAEA TRS 398 Absorbed Dose Determination in External Beam Radiotherapy: An International Code of Practice for Dosimetry based on Standards of Absorbed Dose to Water,” IAEA, Vienna, 2006.

Appendix A

Chamber signal correction factors and calibration factor for ionization chambers [TRS 398]

k_{pol}: Factor to correct the response of an ionization chamber for the effect of a change in polarity of the polarizing voltage applied to the chamber.

$$k_{\text{pol}} = \frac{|M_+| + |M_-|}{2M}$$

where M_+ = chamber signal obtained at positive chamber polarity, M_- = chamber signal obtained at negative chamber polarity, M = chamber signal obtained at the polarity used routinely

$k_{Q,Qo}$: Factor to correct for the difference between the response of an ionization chamber in the reference beam quality Qo used for calibrating the chamber and in the actual user beam quality, Q.

k_s : Factor to correct the response of an ionization chamber for the lack of complete charge collection (due to ion recombination).

$$k_s = a_o + a_1\left(\frac{M_1}{M_2}\right) + a_2\left(\frac{M_1}{M_2}\right)^2$$

where M_1 = chamber signal reading at V_1 (normal operating voltage), M_2 = chamber signal reading at V_2 ($V_2 = V_1/4$), a_0, a_1 and a_2 are constants given in following table.

	Pulsed		
V_1/V_2	a_0	a_1	a_2
2.0	2.337	-3.636	2.299
2.5	1.474	-1.587	1.114
3.0	1.198	-0.875	0.677
3.5	1.080	-0.542	0.463
4.0	1.022	-0.363	0.341
5.0	0.975	-0.188	0.214

k_{TP}: Factor to correct the response of an ionization chamber for the effect of the difference that may exist between the standard reference temperature and pressure specified by the standards laboratory and the temperature and pressure of the chamber in the user facility under different environmental conditions.

$$k_{TP} = \frac{(273.2 + T)}{(273.2 + T_0)} \frac{P_0}{P}$$

where T and P are chamber air temperature (°C) and pressure at the time of measurement. T_0 = 20° C and P_0 = 101.3 kPa

M_Q : Reading of a dosimeter at the quality Q, corrected for influence quantities other than beam quality. Unit: C or rdg.

$$\mathbf{M_Q = M \times k_{pol} \times k_{Q,Qo} \times k_s \times k_{TP}}$$

$N_{D, w, Qo}$: Calibration factor in terms of absorbed dose to water for a dosimeter at a reference beam quality Q_o. The product M_{Qo} $N_{D,w,Qo}$ yields the absorbed dose to water, $D_{w,Qo,}$ at the reference depth z_{ref} and in the absence of the chamber. Unit: Gy/C or Gy/rdg.

$$\boldsymbol{D_{w,Q0} = M_{Q0} \times N_{D,w,Q0}}$$

Appendix B

Sample Plan Assessment Sheet (PAS)

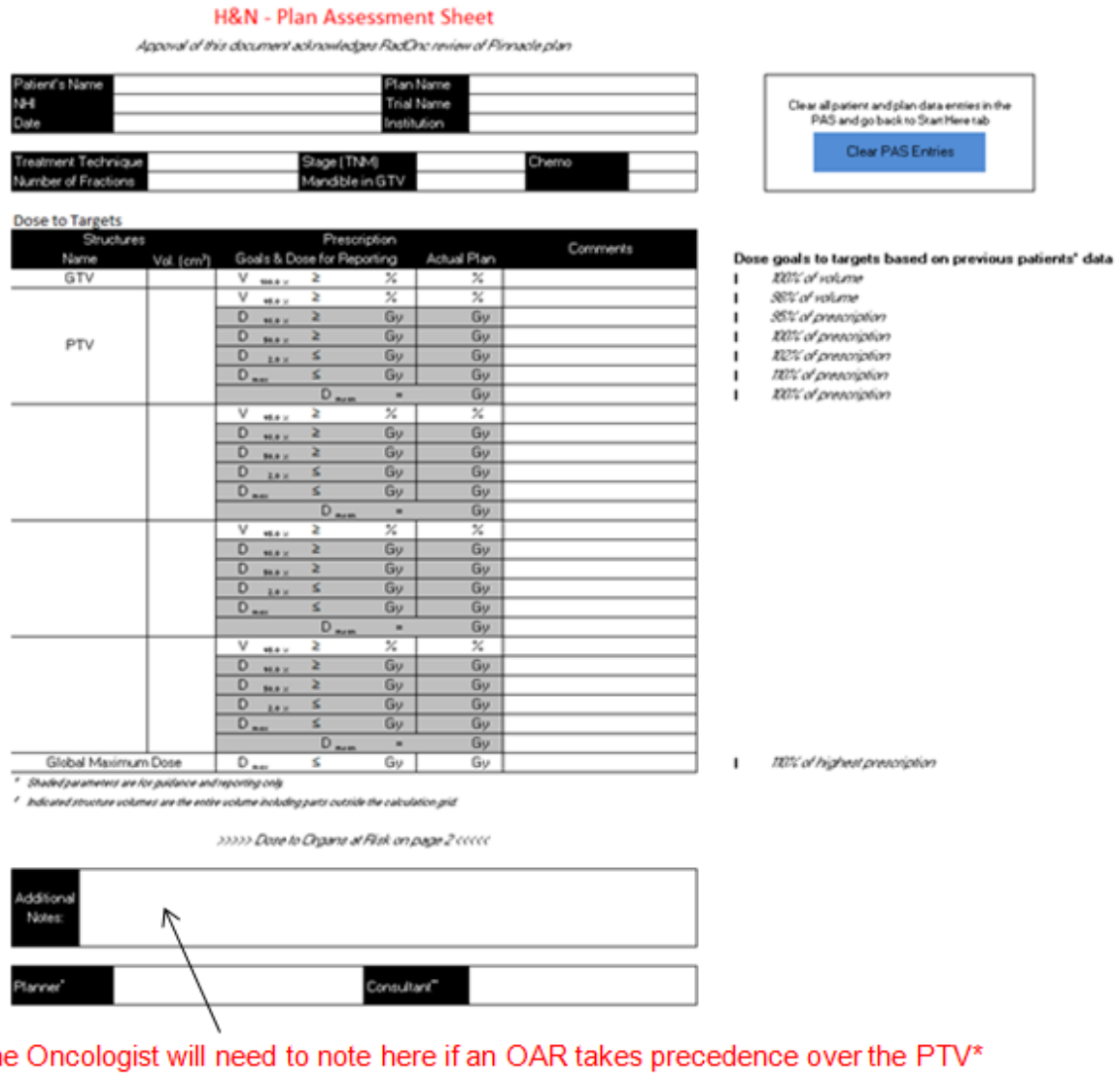

H&N - Plan Assessment Sheet

Approval of this document acknowledges RadOnc review of Pinnacle plan

Patient's Name		Plan Name	
NHI		Trial Name	
Date		Institution	

Treatment Technique		Stage (TNM)		Chemo	
Number of Fractions		Mandible in GTV			

Dose to Targets

Structures		Prescription		
Name	Vol. (cm³)	Goals & Dose for Reporting	Actual Plan	Comments
GTV		V [illegible] ≥ %	%	
PTV		V [illegible] ≥ %	%	
		D [illegible] ≥ Gy	Gy	
		D [illegible] ≥ Gy	Gy	
		D [illegible] ≤ Gy	Gy	
		D_{max} ≤ Gy	Gy	
		D_{mean} =	Gy	
		V [illegible] ≥ %	%	
		D [illegible] ≥ Gy	Gy	
		D [illegible] ≥ Gy	Gy	
		D [illegible] ≤ Gy	Gy	
		D_{max} ≤ Gy	Gy	
		D_{mean} =	Gy	
		V [illegible] ≥ %	%	
		D [illegible] ≥ Gy	Gy	
		D [illegible] ≥ Gy	Gy	
		D [illegible] ≤ Gy	Gy	
		D_{max} ≤ Gy	Gy	
		D_{mean} =	Gy	
		V [illegible] ≥ %	%	
		D [illegible] ≥ Gy	Gy	
		D [illegible] ≥ Gy	Gy	
		D [illegible] ≤ Gy	Gy	
		D_{max} ≤ Gy	Gy	
		D_{mean} =	Gy	
Global Maximum Dose		D_{max} ≤ Gy	Gy	

* *Shaded parameters are for guidance and reporting only*

* *Indicated structure volumes are the entire volume including parts outside the calculation grid*

>>>>> Dose to Organs at Risk on page 2 <<<<<

Additional Notes:	

Planner*		Consultant**	

Clear all patient and plan data entries in the PAS and go back to Start Here tab

Dose goals to targets based on previous patients' data

- *100% of volume*
- *98% of volume*
- *95% of prescription*
- *100% of prescription*
- *102% of prescription*
- *110% of prescription*
- *100% of prescription*
- *110% of highest prescription*

The Oncologist will need to note here if an OAR takes precedence over the PTV

Dose to Organs at Risk

Structures		Constraints		Comments
Name	Vol. (cm^3)	Goals & Dose for Reporting	Actual Plan	
SpinalCord		D_{max} ≤ 45.0 Gy	Gy	
SpinalCord_PRV		D_{max} ≤ 50.0 Gy	Gy	
Brainstem		D_{max} ≤ 54.0 Gy	Gy	
Brainstem_PRV		D_{max} ≤ 60.0 Gy	Gy	
OpticN_L		D_{max} ≤ 50.0 Gy	Gy	
OpticN_L_PRV		D_{max} ≤ 54.0 Gy	Gy	
OpticN_R		D_{max} ≤ 50.0 Gy	Gy	
OpticN_R_PRV		D_{max} ≤ 54.0 Gy	Gy	
Chiasm		D_{max} ≤ 50.0 Gy	Gy	
Chiasm_PRV		D_{max} ≤ 54.0 Gy	Gy	
Eye_L		D_{max} ≤ 50.0 Gy	Gy	
Eye_R		D_{max} ≤ 50.0 Gy	Gy	
Lens_L		D_{max} ≤ 8.0 Gy	Gy	
Lens_R		D_{max} ≤ 8.0 Gy	Gy	
Cochlea_L		D_{max} =	Gy	
Cochlea_R		D_{max} =	Gy	
TemporalLobe		$V_{45.0\ Gy}$ ≤ 1.0 %	%	
		D_{max} ≤ 70.0 Gy	Gy	
Parotid_L		$V_{20.0\ Gy}$ ≤ 50.0 %	%	
		D_{mean} ≤ 26.0 Gy	Gy	
Parotid_R		$V_{20.0\ Gy}$ ≤ 50.0 %	%	
		D_{mean} ≤ 26.0 Gy	Gy	
SMG_L		D_{mean} =	Gy	
SMG_R		D_{mean} =	Gy	
Lips		D_{mean} ≤ 20.0 Gy	Gy	
OralCavity		D_{mean} ≤ 42.0 Gy	Gy	
OralCavity-PTV		D_{mean} ≤ 30.0 Gy	Gy	
Constrictors		D_{mean} ≤ 63.0 Gy	Gy	
Constrictors-PTV		$V_{50.0\ Gy}$ ≤ 33.0 %	%	
		$V_{60.0\ Gy}$ ≤ 15.0 %	%	
		D_{mean} ≤ 45.0 Gy	Gy	
GSL		D_{mean} ≤ 20.0 Gy	Gy	
Oesophagus		D_{mean} ≤ 30.0 Gy	Gy	
BrPlexus_L		D_{max} ≤ 66.0 Gy	Gy	
BrPlexus_L_PRV		D_{max} =	Gy	
BrPlexus_R		D_{max} ≤ 66.0 Gy	Gy	
BrPlexus_R_PRV		D_{max} =	Gy	
Mandible		$V_{66.0\ Gy}$ ≤ 1.0 %	%	
		D_{max} ≤ 70.0 Gy	Gy	
Mandible_L		$V_{66.0\ Gy}$ ≤ 1.0 %	%	
		$V_{50.0\ Gy}$ =		
		D_{max} ≤ 70.0 Gy	Gy	
Mandible_R		$V_{66.0\ Gy}$ ≤ 1.0 %	%	
		$V_{50.0\ Gy}$ =		
		D_{max} ≤ 70.0 Gy	Gy	
VocalCords		D_{mean} ≤ 26.0 Gy	Gy	

' Shaded parameters are for guidance and reporting only.

' Indicated structure volumes are the entire volume including parts outside the calculation grid.